

What drives F_{yw} variations Towards a conceptualization of the hydrological processes behind changes of young water fraction with elevation in Alpine: a focus on mountainous alpine catchments?

Alessio Gentile¹, Davide Canone¹, Natalie Ceperley⁴, Davide Gisolo¹, Maurizio Previati¹, Giulia Zuecco³, Bettina Schaepli^{2,4}, and Stefano Ferraris¹

¹Interuniversity Department of Regional and Urban Studies and Planning (DIST), Politecnico and Università degli Studi di Torino, Torino, Italy

²Institute of Earth Surface Dynamic (IDYST), Faculty of Geosciences and Environment (FGSE), University of Lausanne, Lausanne, Switzerland

³Department of Land, Environment, Agriculture and Forestry (TESAF), University of Padova, Legnaro, Italy

⁴Institute of Geography (GIUB) and Oeschger Centre for Climate Change Research (OCCR), University of Bern, Bern, Switzerland

Correspondence to: Bettina Schaepli (bettina.schaepli@giub.unibe.ch)(bettina.schaepli@giub.unibe.ch)

Abstract. The young water fraction (F_{yw} / F_{yw}^*), defined as the fraction of catchment outflow with transit times of less than about 2-3 months, is increasingly used in hydrological studies, replacing that exploit the widely-used Mean-Transit-Time (MTT), which is subject to aggregation error potential of isotope tracers. The use of this new metric in catchment intercomparison studies is helpful to understand and conceptualize the relevant processes controlling catchment's hydrological function-catchment functioning. Past work has works have shown the remarkable and counterintuitive surprising evidence that steep (and generally high elevation) mountainous catchments worldwide reveal small F_{yw} yield low F_{yw}^* . These low values. However, the topographic slope only have been partially explains the observed F_{yw} variance, and the explained by isolated hydrological processes, including deep vertical infiltration and long groundwater flow paths. However, a harmonious framework illustrating the relevant mechanisms hidden behind this lowering with slope remain basically unclear leading to a low F_{yw}^* in mountainous catchments is missing.

The main aim of this paper is to investigate-give an overview of what drives F_{yw} / F_{yw}^* variations with according to elevation in Alpine catchments, thus clarifying why F_{yw} is low it generally decreases at high altitudes. In elevation. For this regard purpose, we use assembled a dataset composed data set of 27 study catchments, located both in across Switzerland and in Italy, that we categorize as rainfall-dominated, hybrid or for which F_{yw}^* values are available or have been calculated. We assume that this decrease can be explained by the groundwater storage potential, quantified by the areal extent of Quaternary deposits over a catchment (F_{gd}), and the low-flow duration (LFD) throughout the period of isotope sampling (PoS). In snow-dominated according to a proposed formal classification scheme that considers both a common-used monthly streamflow ratio and the snow cover regime. We analyze three not previously investigated variables that could potentially explain the F_{yw} -elevation gradients: the systems, LFD is strictly related to the snowpack persistence, quantified from Sentinel-2 L2A

35 ~~satellite images through the average~~ fractional snow cover area (F_{SCA}), ~~the fraction of quaternary deposits (F_{qd}), and the~~
~~fraction of). The drivers under study are directly or indirectly related to the catchment storage contribution to the stream,~~
~~that we quantify applying a cutting-edge baseflow separation method to the discharge time series of the study sites and~~
~~estimating the average baseflow fraction (F_{bf}). We also consider a fourth variable, namely the Winter Flow Index (WFI), for~~
40 ~~comparing our results about the groundwater contribution to streamflow with those of previous scientific publications.) over~~
~~the PoS.~~

Our results suggest that ~~unconsolidated sediments~~Quaternary deposits could potentially play a role in modulating F_{yw} F_{yw}^*
elevation gradients via their capacity to store groundwater, but ~~a future confirmation with further, more detailed geological~~
~~information, such as the portion of fractured bedrocks, would be desirable for a complete picture of the role of geology.~~
~~Based on our analysis concerning the F_{SCA} , is necessary. LFD measures the proportion of PoS in which the stream is~~
45 ~~sustained and dominated by stored (old) water coming from the catchment storage. Accordingly, our results reveal that the~~
~~increase of LFD at high elevations, to a large extent driven by the persistence of winter snowpacks and the simultaneous lack~~
~~of a liquid water input to the catchments, results in lower F_{yw}^* . In our data set F_{bf} reveals a strong complementarity with~~
 F_{yw}^* , suggesting that the latter could be estimated as $F_{yw}^* \simeq 1 - F_{bf}$ for catchments in which stable water isotopes
measurements are not available.

50 ~~As a conclusion, we develop a perceptual model that explains how the increasing duration of the snowpack promotes a~~
~~progressive emptying of the groundwater storage during winter, thereby increasing the streamwater age, while ephemeral~~
~~snowpack generally favors rapid flow paths that increase F_{yw} . Finally, our work highlights that F_{bf} , considered as a~~
~~proxy integrates all the results of our analysis to describe a framework for groundwater flow, is roughly the one's~~
~~complement of F_{yw} . In harmony with the model, we find high F_{bf} during all low-flow periods, which underlines that~~
55 ~~streamflow is mainly sustained by groundwater in such flow conditions. For catchments where the winter low-flow period is~~
~~long compared to the summer high-flow period, this results in low F_{yw} . how hydrological processes control F_{yw}^* according to~~
~~elevation, laying the foundations for an improvement of the theory-driven models.~~

In conclusion, our data set suggests that F_{bf} is the best explanatory variable of F_{yw} elevation gradients in Alpine catchments,
implying the key role of major groundwater storages that, with the increasing snowpack duration, are actively involved in
60 streamflow generation processes.

1 Introduction

~~Alpine~~Mountainous alpine catchments are often assumed to generate a high share of rapid surface or subsurface runoff
due to the presence of exposed bedrock and steep landscapes, ~~consequently~~. Consequently, the role of groundwater storage
in high-elevation catchments has been often neglected (Hayashi, 2020). However, early work in the Swiss Alps showed that
65 ~~high celerity is caused by the release of groundwater to the stream, so that the streamflow is older than the annual~~
~~snowmelt~~On the contrary, multiple worldwide studies quantified a considerable groundwater input to streamflow in high

mountain catchments using tracer or water balance (Martinez, 1975). This corresponds to results obtained through stable-isotope based hydrograph separation performed in 101 studies worldwide that revealed that more than half of streamflow is composed of groundwater even during no-rain and no-snowmelt periods (Jasechko, 2019). To date, it is well known that the age of water stored in catchments is well beyond the annual timescale and that it plays a key role in streamflow generation processes (McDonnell, 2017; Jasechko, 2019). In this regard, the hydrological community expressed the need for better understanding of transit time distributions in the terrestrial water cycle (Blöschl et al., 2019).

The study of water age is crucial for predicting the timing of nutrient cycles and pollutant transport since water age and solute dynamics can be coupled (Jasechko et al., 2016; Benettin et al., 2017). However, water age quantification is not

straight forward. Kirchner (2016a, b) proposed a new metric to quantify water age at the catchment scale: the young water fraction (F_{yw}), defined as the fraction of catchment outflow with transit times of less than roughly 0.2 years (Kirchner, 2016a). It can be conveniently inferred from the dampening effect that a catchment has on the seasonal cycle of stable water isotopes in precipitation, i.e. by estimating the amplitude ratio of the seasonal cycle of stable water isotopes in streamflow to that of precipitation (Kirchner, 2016a). The F_{yw} concept has rapidly supplanted the similar metric, Mean Transit Time (MTT), because it has the advantage of being free from the aggregation errors inherent to MTT . The F_{yw} is also an informative proxy of a catchment's hydrological function, in terms of water partitioning and release (Stockinger et al., 2019). Therefore, this new metric is useful for catchment intercomparison studies to analyze the main hydro-climatic and landscape characteristics that influence the transit times of water (von Freyberg et al., 2018). Indeed, some studies have already tried to find a relationship between young water fractions and catchment characteristics. von Freyberg et al. (2018) found that young water fractions of 22 Swiss catchments are positively correlated (with statistical significance) with selected hydro-climatic indices and the fraction of saturated area, suggesting that F_{yw} depends on catchment wetness which promotes rapid flow paths.

Interestingly, the analysis by von Freyberg et al. (2018) revealed that the young water fraction is positively correlated with mean catchment elevation, but only when the 5 high elevation, snow dominated catchments are omitted from the analysis.

Indeed, Ceperley et al. (2020), who compared the F_{yw} from three additional high elevation catchments to the original dataset of von Freyberg et al. (2018), observe a drop of F_{yw} above 1500 m a.s.l., to which we refer hereafter as F_{yw} -reset. In line with these findings, a recent study estimated F_{yw} for 24 catchments in Germany and observed the smallest values in mountainous landscapes (Lutz et al., 2018).

This F_{yw} -reset is partially consistent with the counterintuitive outcomes of Jasechko et al. (2016) whose work reveals that young streamflow is less prevalent in steep (and generally high) landscapes. They explain this by a consistent deep vertical infiltration component for such steep high elevation catchments (Jasechko et al., 2016). However, even if the topographic gradient is correlated with the young water fraction in the 254 watersheds data set of Jasechko et al. (2016), the relationship is relatively scattered, leaving a large portion of variance unexplained and suggesting that other variables can play a key role in reducing F_{yw} according to slope steepness or with elevation (Jasechko et al., 2016).

100 Comparing different F_{yw} estimation methods in presence of snow in the Swiss and Italian Alps, Ceperley et al. (2020) observed that high Alpine catchments reveal low F_{yw} . Therefore, the snow storage could have a role in decreasing the young water fraction. The elevation of 1500 m a.s.l., above which we have the F_{yw} -reset, has been previously identified as corresponding to the transition between intermittent and seasonal snow cover (Santos et al., 2018). However, it is unclear if the snow cover dynamics can lead to a more efficient groundwater recharge, consequently reducing or increasing the young streamflow reaching the stream (Ceperley et al., 2020).

105 Tracer or water balance methods are powerful tools to quantify groundwater contribution to rivers and multiple worldwide studies have estimated the considerable groundwater input to streamflow in high mountain catchments using such methods (Somers and McKenzie, 2020). Several catchments studies located in the Rocky Mountains and Andes mountain ranges show that remarkable fractions, on average, about 47% of groundwater annually sustains the streamflow (Saberli et al., 2019; Somers et al., 2019; Carroll et al., 2018; Harrington et al., 2018; Cowie et al., 2017; Baraer et al., 2015; Gordon et al., 2015; Frisbee et al., 2011; Liu et al., 2004; Clow et al., 2003; Baraer et al., 2009) (Saberli et al., 2019; Somers et al., 2019; Carroll et al., 2018; Harrington et al., 2018; Cowie et al., 2017; Baraer et al., 2015; Gordon et al., 2015; Frisbee et al., 2011; Liu et al., 2004; Clow et al., 2003; Baraer et al., 2009). This result is similar results are also found in the Himalayas (49%) and the Alps mountain ranges (48%) (Chen et al., 2018; Engel et al., 2016; Käser and Hunkeler, 2016; Williams et al., 2016; Wilson et al., 2016; Andermann et al., 2012). To date, it is well known that the age of water stored in catchments is well beyond the annual timescale and that it plays a key role in streamflow generation processes (McDonnell, 2017; Jasechko, 2019). The study of water age is crucial for predicting the timing of nutrient cycles and pollutant transport since water age and solute dynamics are closely coupled (Li et al., 2021). However, water age quantification is not straight forward. There is however still a lack of understanding regarding the mechanisms that lead to a dynamic storage contribution to streamflow (Kirchner, 2003) and, consequently, how this contribution impacts the young water fraction.

120 Kirchner (2016a, b) proposed a new metric to quantify the share of catchment outflow with transit times lower than roughly 0.2 years or 2-3 months: the young water fraction. This metric can be conveniently inferred from the dampening effect that a catchment has on the seasonal cycle of stable water isotopes in precipitation, i.e. by estimating the ratio of the amplitudes of the seasonal cycles of stable water isotopes in streamflow and in precipitation (Kirchner, 2016a). In this method, the seasonal cycle of stream water isotope measurements is modelled using a sine wave that can be flow-weighted or not, using as weights the discharge measured at the moment of sampling (von Freyberg et al., 2018). Isotopes measured in precipitation can be modelled with a sine function weighted according to the volume of precipitation, to reduce the influence of low-precipitation periods and to account for temporally aggregated rainfall samples (von Freyberg et al., 2018). Flow-weighted fits to the seasonal tracer cycles predict the flow-weighted average young water fraction (F_{yw}^*) in streamflow, while unweighted fits to the seasonal tracer cycles predict the unweighted one (F_{yw}) (Kirchner, 2016b). Gallart et al. (2020a) recently highlighted the advantages of the flow-weighted analysis to compensate for subsampled high-flow periods, thus

125
130

reducing the underestimation of the young water fraction. Hereafter, we will use the symbol '*' for referring to a flow-weighted variable, in order to be consistent with previous studies (von Freyberg et al., 2018; Gallart et al., 2020a).

F_{yw}^* is increasingly used in hydrological studies because it has the advantage of being free from the aggregation errors inherent to Mean Transit Time (MTT) estimates obtained through the classical convolution approach (Kirchner, 2016a). Even more so, F_{yw}^* is an informative descriptor of catchment hydrological functions, of nutrients cycles and of pollutant transport (Stockinger et al., 2019; Benettin et al., 2017; Jasechko et al., 2016). Therefore, this new metric is useful for catchment intercomparison studies to find what are the main hydro-climatic and landscape characteristics that drive the transit times of water lower than 2-3 months. Indeed, past works have tried to study the relationship between F_{yw}^* and catchment characteristics. von Freyberg et al. (2018) found that young water fractions of 22 Swiss catchments are positively correlated (with statistical significance) with selected hydro-climatic indices and with the fraction of saturated area, suggesting that F_{yw}^* depends on catchment wetness, which promotes rapid flow paths. Interestingly, in their data set, a statistically significant positive correlation with elevation was obtained after removing from their analysis the five snow-dominated catchments, which revealed the smallest F_{yw}^* values (von Freyberg et al., 2018). Likewise, Lutz et al. (2018) estimated F_{yw}^* for 24 catchments in Germany and found the smallest values for higher-elevation sites. These results are partially consistent with those of Jasechko et al. (2016): based on the analysis of 254 watersheds worldwide, their work revealed a reduction of F_{yw}^* in mountainous, steeper terrains. This could be related to deep vertical infiltration caused by fractures generated by high rock stress in complex terrain morphologies or by freely draining soils (i.e., cambisols and luvisols), both associated to high-elevation environments (Lutz et al., 2018; Jasechko et al., 2016; Gleeson et al., 2014). In addition, the higher the topographic roughness is, the longer are the flow paths, with a consequent rise of transit times (Gleeson and Manning, 2008; Frisbee et al., 2011; Jasechko et al., 2016). Despite of these studies, there is still a lack of a harmonious framework of how the relevant drivers and hydrological processes in mountainous catchments lead to a small percentage of young water at high elevation, leaving this result basically unclear.

An early work in the Swiss Alps shows that high celerity is caused by massive meltwater infiltration that pushes out groundwater reserves: streamflow following snowmelt is older than meltwater infiltrated in the current year (Martinec, 1975). The resulting effect on water partitioning between the surface and the subsurface should be analyzed considering the temporal concentration of water input on the snowmelt period, but this remains largely unexplored to date (Rey et al., 2021). Despite of this lack of studies on water partitioning during snowmelt, several studies have demonstrated the pivotal role of snowmelt in recharging groundwater during summer in high-elevation environments (Hayashi, 2020; Cochand et al., 2019; Du et al., 2019; Flerchinger et al., 1992).

From a water storage perspective, and thus from a water age perspective, snowpack storage and groundwater storage can be considered as a single entity: they both constitute catchment storage. Therefore, the analytical estimation of F_{yw}^* must reflect this "conceptual" decision of considering the snowpack storage as part of the catchment storage or not. This point has been previously addressed by von Freyberg et al. (2018): if total precipitation is considered as catchment input (what can be called

165 the direct input case), the snowpack is implicitly considered as part of the catchment storage and F_{yw}^* results from the combination of snowpack and subsurface storage. In this direct input case, F_{yw}^* is computed from the amplitudes of the seasonal cycles of stable isotopes of water in precipitation (A_p) and in streamflow (A_s^*). If total liquid water input (composed of rainfall and snowmelt, sometimes called equivalent precipitation) is considered as catchment input, F_{yw}^* is computed based on the amplitudes of the cycles in equivalent precipitation (A_{peq}) and in streamflow (A_s^*). This F_{yw}^* value then results from subsurface storage alone, since snowpack storage is excluded from the catchment storage (von Freyberg et al., 2018). If F_{yw}^* is estimated using a direct input setting (i.e., total precipitation directly), F_{yw}^* is expected to be smaller since the catchment storage is larger (von Freyberg et al., 2018). Also, Ceperley et al. (2020) investigated the role of water input from snow in F_{yw}^* estimation, concluding that the low values in high alpine snow-dominated catchments result from a combination of snow cover effects and the storage in the subsurface. In the present work, the main aim is not to focus on how the snowpack affects F_{yw}^* estimation in a single catchment, as this was treated in previous works (von Freyberg et al., 2018; Ceperley et al., 2020), but to investigate the hydrological processes (also related to the snowpack storage) that lead to changes in F_{yw}^* between catchments located at different elevations, focusing on high-elevation alpine catchments. Some authors have revealed the possibility of quaternary deposits (e.g., talus, moraine, alluvium) to store groundwater in high-elevation alpine catchments (Arnoux et al., 2021; Hayashi, 2020; Christensen et al., 2020). The stored water in these deposits can in fact sustain streamflow during the low-flow period (Hayashi, 2020; Arnoux et al., 2021). Moreover, recent streamflow data-based and model-based studies in the Swiss Alps point towards important mobile groundwater storage in high elevation catchments, which could be related to quaternary deposits: e.g., moraines, alluvium, and talus (Staudinger et al., 2017; Coehand et al., 2019; Arnoux et al., 2021). Therefore, it is necessary to understand the capability of unconsolidated sediments of storing high mountain groundwater and how this geology influences the amount of young water reaching the stream.

185 Accordingly, we study here a new set of hydrological variables to gain new insights into the F_{yw} along elevation gradients: the fractional snow cover area (F_{SCA}), the fraction of quaternary deposits (F_{qd}) and the fraction of baseflow (F_b), defined in detail in Sections 3.4 and 3.5. We also consider a fourth index, namely the Winter Flow Index (WFI), for testing consistency of our results with those of a past study (Arnoux et al., 2021) that used this index to quantify the groundwater contribution to streamflow.

190 In the following, we first classify the study catchments, described in Section 2, into three hydro-climatic regimes proposing a new criterion of classification (Section 3.3). Then, we study the correlation of the selected hydrological variables with the young water fraction (Sections 4.3.1, 4.3.2, 4.3.3) and we finally bring these results back to the ongoing scientific discussion of F_{yw} (Section 5).

195 as supported by the strong positive correlation found by Arnoux et al. (2021) between the fraction of quaternary deposits and the Winter Flow Index (a low-flow indicator reflecting the groundwater contribution to the stream) for 13 alpine catchments. During winter, the period without liquid water input can last 6 months or more in high elevation catchments. Such sustained

flow during long periods points towards important amounts of stored water (or old water) that are well connected to the stream network and thereby remains accessible throughout the low flow period. (Somers et al., 2019).

200 To further discuss the role of low flow in F_{yw}^* estimation, let's first consider that F_{yw}^* can be estimated based on the flow-weighted average of young water fractions (Kirchner, 2016b):

$$F_{yw}^* = \frac{A_S^*}{A_P} \approx \frac{\sum_{i=1}^n Q(t_i) F_{yw}(t_i)}{\sum_{i=1}^n Q(t_i)}, \quad (1)$$

where n is the number of time-steps (e.g., days) in the period of isotope sampling, PoS, $Q(t_i)$ is the discharge at the time t_i (e.g., daily discharge), $F_{yw}(t_i)$ is the young water fraction at the time t_i (e.g., daily young water fraction). As is clear from Eq.

205 (1), F_{yw}^* becomes low if either $F_{yw}(t_i)$ is low for high flows or if $F_{yw}(t_i)$ is very low for many time steps or both. The low-flow periods correspond to the recession periods in which there is no new rainfall or meltwater input in the catchments. Thus, during these periods, the catchment storage releases stored water (or old water) to the stream sustaining the streamflow (Hayashi, 2020). Thus, we can anticipate that low $Q(t_i)$ values imply low $F_{yw}(t_i)$ values. Accordingly, the proportion of the low-flow period during a specified time-window should reduce the amount of young water reaching the stream during that

210 time-window. Nevertheless, the $F_{yw}(t_i)$ is higher during high flow (wet) periods (von Freyberg et al., 2018; Wilusz et al., 2017; Gallart et al., 2020b). Thus, the overall effect of the proportion of low-flow and high-flow periods upon F_{yw}^* remains a priori unclear. It is however tempting to think that the duration of low-flow period or the share of baseflow could explain F_{yw}^* changes at different elevations (since both low-flow duration and the share of baseflow change with elevation). In addition, in high-elevation, snow-dominated catchments the snowpack persistence is the main driver of low-flow duration,

215 since the low-flow period in such environments corresponds to the presence of the seasonal snowpack (corresponding to an absence of liquid water input), while the high-flow period is generally snowmelt-driven. Such snowmelt generally occurs in late spring or summer and it is likely to be older than 2-3 months (because melted snow fell more than 3 months before the onset of snowmelt). As a result, summer discharge would mainly consist of old water: either of current snowmelt that reaches the stream via faster surface or subsurface flow paths or old snowmelt (main component of groundwater storage) pushed out in the stream by infiltrated rainwater or meltwater. Of course, part of the snowpack could release young water, but this should be a minor component in catchments with a seasonal snowpack. In contrast, in catchments with an ephemeral snowpack, it is common to observe intermittent winter snowmelt that is likely younger than 2-3 months: snowmelt is temporally close to snowfall. In this case streamflow receives relatively more young water from short-lived snowpacks. However, it is still unclear if seasonal or ephemeral snow cover dynamics can affect the F_{yw}^* (Ceperley et al., 2020).

225 A special focus of our work is on variables that were not previously considered for explaining elevation gradients of young water fractions. We namely exclude catchment size, annual precipitation, bedrock porosity, pasture cover, open water cover that have been discussed and shown to have little correlation in the work of Jasechko et al. (2016).

A special case in terms of explanatory variables is mean annual precipitation: Jasechko et al. (2016) in their worldwide study did not observe any significant correlation between the F_{yw}^* and annual precipitation. Lutz et al. (2018) found, based on 24

230 catchments in Germany, that F_{yw}^* decreases with increasing mean annual precipitation. In contrast, in the relatively wet
rainfall-dominated and hybrid catchments studied by von Freyberg et al. (2018), F_{yw}^* was shown to increase with
precipitation, which in turn both increase with elevation. In their study, discharge (unsurprisingly correlated with
precipitation) was considered as a proxy of catchment wetness, which favours rapid flow paths and thereby increases F_{yw}^*
(von Freyberg et al., 2018). In snow-dominated systems, the use of mean annual precipitation as a proxy for catchment
235 wetness could be misleading because the seasonal snowpack leads to a very dry period of the year despite the high *solid*
water input. In other words, the temporal concentration of the liquid water input is the relevant variable. Indeed, the
saturation of the system (i.e., high wetness conditions) can be observed also when the annual precipitation is low if a large
volume of water (stored in the snowpack) is released in a relatively concentrated time interval. Indeed, despite
precipitations, and correspondingly discharges, are relatively higher in snow-dominated than in rainfall-dominated
240 catchments, F_{yw}^* is generally lower in snow-dominated systems that are potentially wetter than rainfall-dominated ones. This
suggests that the only precipitation can only partially explain the variations of F_{yw}^* and that other variables should be put
under observation.
Accordingly, we omit here total annual precipitation as explanatory variable of low F_{yw}^* in snow-dominated catchments (but
we consider precipitation for rainfall-dominated and hybrid catchments) and study a new set of hydrological variables to
245 gain new insights into F_{yw}^* along elevation gradients: the fraction of Quaternary deposits (F_{qd}), the average fraction of
baseflow (F_{bf}), the low-flow duration (LFD) and the average fractional snow cover area (F_{SCA}), defined in detail in Section
3.2 and Section 3.3. In the following, we first describe the data set (Section 2). Then, we present the correlation analysis of
the selected hydrological variables with F_{yw}^* and we bring these results back into the ongoing scientific discussion of F_{yw}^*
(Sections 4.1, 4.2, 4.3, 4.4, 4.5).

250 2 Study sites

~~In this work we~~ analyze 27 study catchments located both in Switzerland and Italy (Table S1, Fig. 1) and
~~integrate~~integrating observations from multiple published existing ~~datasets~~data sets (25 catchments) with new additional
observations (2 catchments) (Fig. 1). Geomorphological and hydro-climatic characteristics of the study sites are reported in
Table 1.

255 2.1 Existing dataset

Initial, we integrate the 22 Swiss catchments studied by von Freyberg et al. (2018) with the three Alpine catchments (Vallon
de Nant, Noce Bianco at Pian Venezia and Bridge-Creek-Catchment) investigated by Ceperley et al. We assembled the 22
Swiss catchments studied by von Freyberg et al. (2018) with the three alpine catchments investigated by Ceperley et al.
(2020) into a single dataset. Time series of both $\delta^3\text{H}$ and $\delta^{18}\text{O}$ in streamflow and precipitation for the 22 Swiss catchments
260 are reported and described by Staudinger et al. (2020). Furthermore, 21 out of the 22 Swiss catchments were also considered

in a previous study (which did not consider the Alp catchment) that analyzed the variation of the catchment water storage with elevation (Staudinger et al., 2017). In turn, daily isotope measurements for the Alp (ALP) catchment and its two tributaries, Erlenbach (ERL) and Vogelbach (VOG) catchments, were thoroughly described by von Freyberg et al. (2022). Two high elevation catchments among the 22, namely Dischmabach (DIS) and Ova da Cluozza (OVA), were also investigated in previous studies for climate change impact predictions, low flow analysis and for understanding the role of quaternary deposits and groundwater in their hydrological functioning (Addor et al., 2014; Staudinger and Seibert, 2014; Staudinger et al., 2015; Jenicek et al., 2018; Arnoux et al., 2021). Among the catchments analyzed by Ceperley et al. (2020), the reader is referred to Michelon et al. (2022) for further information about the tracer-based dynamics of the Vallon de Nant (VdN) catchment and to Carturan (2016), Carturan et al. (2013, 2014, 2016, 2019), Zuecco et al. (2019) for glaciological, hydrological and meteorological information about the Noce Bianco at Pian Venezia (NBPV) catchment. Additional details for the dolomitic Bridge Creek Catchment (BCC) are available in the work of Zuecco et al. (2018, 2019), Guastini et al. (2019) and Penna et al. (2016, 2017).

2.2 — Additional dataset

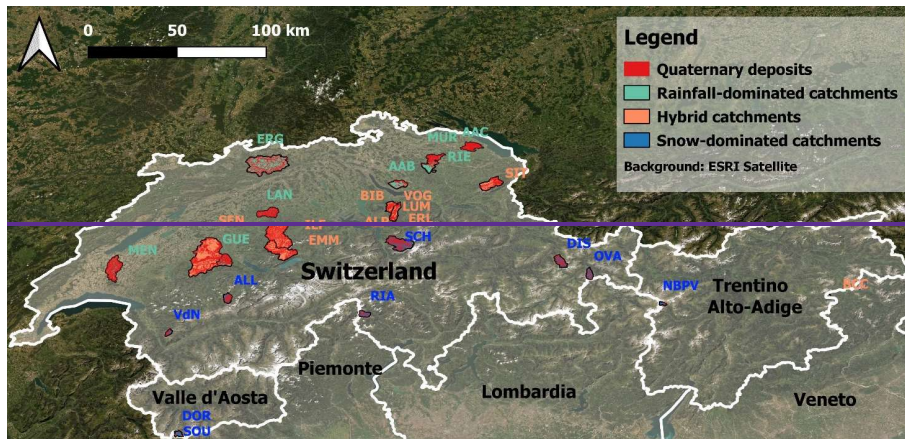
We consider two additional high elevation catchments located near the Nivolet Pass (Valsavaranche, Aosta Valley, Italy) in a high elevation grassland within the Gran Paradiso National Park territory (Gisolo et al., 2022). The mainstream is the Dora del Nivolet. Hereafter we refer to this catchment simply as “Dora” (DOR). DOR has a catchment area of 17 km² and its elevation ranges from 2390 to 3430 m a.s.l. Average annual precipitation in the period 2017-2021 was 2164 mm. It experiences a snow-dominated hydro-climatic regime with the snowpack generally persisting from mid-November to mid-May when the snowmelt starts. Since the snowpack melts during the growing season, it uncovers a typical alpine meadow home to plant species including *Gentiana Lutea* L., *Juniperus Communis* L., *Vaccinium Myrtillus* L., *Salix Alpina* Scop. and *Trifolium Alpinum* L. The lithology of DOR is dominated by gneiss. Bedrock emerges at high elevations, while at medium elevations the talus dominates. At lower elevations we find the alpine meadow, characterized by peat substrate, through which the mainstream flows. We monitor precipitation every month with a rain gauge located at roughly 2560 m a.s.l. We measure streamflow continuously (10 min timestep) at the DOR outlet point and in a lateral subcatchment, on the left bank of the mainstream, using piezo-resistive multi-sensors. We call this lateral subcatchment “Souree” (SOU), since it is characterized by water emerging from underground. The SOU subcatchment extends for roughly 0.16 km² and its elevation ranges from 2390 to 2790 m a.s.l. Water samples for isotopic analysis are collected of both bulk precipitation and streamwater at a monthly time resolution. Specifically, precipitation samples were collected using a double rain and snowfall isotope sampler installed on a pole 3.7 m high, near the rain gauge, while streamwater was sampled manually (Fig. S1). All precipitation and streamwater samples were analyzed with laser spectroscopy at the Forest Hydrology laboratory of University of Padova.

2.3 — Complete dataset

The von Freyberg et al. (2018) dataset includes catchments with areas between 0.7 and 351 km² and mean elevations between 472 and 2369 m a.s.l. Average annual precipitation in these catchments ranges from 887 to 2615 mm. With the data added here, the entire dataset now covers areas between 0.14 and 351 km² and has mean elevations between 472 and 3049 m a.s.l. Specifically, the additional 5 catchments added to the initial dataset of von Freyberg et al. (2018) allow analysis to explore the high elevation (i.e., > 1500 m a.s.l.) regions that were previously poorly represented. Furthermore, the complete dataset now includes case studies from five different Alpine regions, including the Northern part of the Swiss Alps, the Southern Swiss Alps (Alpi Ticesini), the Western Italian Alps (Alpi Graie), the Rätische Alpen and the Dolomites. This represents a good range of geologies as well as of climatic conditions, as visible from Table 1.

Like von Freyberg et al. (2018), we classify the catchments in the three hydro-climatic regimes (snow-dominated, hybrid and rainfall dominated) proposed by Staudinger et al. (2017), but we introduce a new formal criterion of classification (see Section 3.3).

The geographical framework of the selected catchments is illustrated in Fig. 1 and their geomorphological and climatic characteristics are reported in Table 1.



(Vallon de Nant, Noce Bianco at Pian Venezia and Bridge Creek Catchment) into a single data set. Hereafter we refer to these catchments with the ID reported in the above-mentioned published papers (Table 1). We also consider two additional high-elevation catchments located near the Nivolet Pass (Valsavaranche, Aosta Valley, Italy) (Gisolo et al., 2022). In this Alpine environment, we monitor the mainstream, called “Dora del Nivolet”, and a secondary river called “Source”. Hereafter

we refer to these catchments with the ID: DOR and SOU, respectively. A detailed description of the DOR and SOU catchments is reported in the Supplementary Material.

The von Freyberg et al. (2018) data set includes catchments with areas between 0.7 and 351 km² and mean elevations between 472 and 2369 m a.s.l. With the five catchments added here, the complete data set covers areas between 0.14 km² and 359 km² and has mean elevations between 472 and 3049 m a.s.l. The average precipitation is comprised between 61.3 mm month⁻¹ and 168.7 mm month⁻¹ while mean discharge is comprised between 28.6 mm month⁻¹ and 138.9 mm month⁻¹. The average slope ranges from 4° to 34°, and our study sites reveal an increase of steepness with elevation (Fig.2a, Fig.2b). Precipitation increases with elevation until 1500 m a.s.l. and it decreases for higher elevations (Fig. 2c, Fig. 2d), highlighting a change of precipitation regime as described by previous studies (Santos et al., 2018). The five catchments added to the initial data set of von Freyberg et al. (2018) allow the analysis to explore the high-elevation regions (average elevation > 1500 m a.s.l.) that were previously poorly represented. Most of the study catchments reveal a sedimentary bedrock, but also dolomitic and metamorphic bedrocks, characteristic of high-elevation sites, are included in our data set. Moreover, the presence of unconsolidated Quaternary deposits is widespread among our study catchments: only two catchments (BCC and SOU) do not reveal this type of geology. The complete data set now explores case studies from the Swiss plateau and Prealpine area, from the Jura and from five different Alpine regions, including the Northern part of the Swiss Alps, the Southern Swiss Alps (Alpi Ticinesi), the Western Italian Alps (Alpi Graie), the Rätische Alps and the Dolomites. In summary, this represents a good range of geologies as well as of climatic conditions.

In order to be consistent with previous studies (von Freyberg et al., 2018; Staudinger et al., 2017), we classify the 23 Swiss catchments according to the hydro-climatic regimes proposed by Staudinger et al. (2017) which group the regimes defined by Weingartner and Aschwanden (1992) in three categories: rainfall-dominated (R), hybrid (H) and snow-dominated (S). For the four Italian catchments, where the aforementioned classification schemes cannot be rigorously applied, we use that proposed by Stoelzle et al. (2020). This classification scheme is based on mean and maximum catchment elevation, periods of typical low-flow, snow onset and begin of snowmelt and was already used by Stoelzle et al. (2020) to classify catchments outside the Swiss borders (e.g., German catchments). According to this classification scheme, the four Italian catchments (DOR, SOU, BCC and NBPV) are all categorized as snow-dominated (S). The classification of BCC is also consistent with the one given in a previous study without considering the application of a formal classification scheme (Penna et al., 2016). Across the three considered streamflow regimes, a shift of the monthly hydrograph peak (computed using discharge data in the PoS) from winter to summer months is observed (Fig. 3); this “flow peak-shifting” is a clear sign of the increasing predominance of snowmelt in the streamflow generation processes. Our data set includes NBPV, whose area is 42% glacier-covered and consequently shows a characteristic glacier-dominated streamflow regime with a monthly peak in late summer. Thus, NBPV may belong to a fourth category of glacier-dominated catchments, for which the effect of glacier-melt on F_{vw}^* cannot be neglected, and this was partially discussed by Ceperley et al. (2020). In our data set, also the Dischmabach (DIS)

and the Vallon de Nant (VdN) catchments are 2% and 3% glacier-covered, but we assume that the effect on F_{319}^* is negligible.

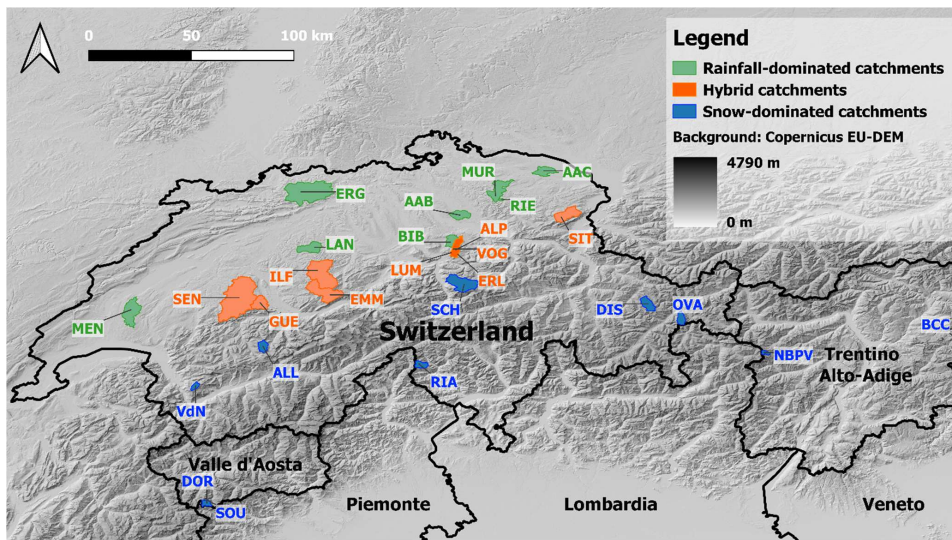


Figure 1.1 Location of the 27 study catchments with indication of hydro-climatic regime and quaternary deposits coverage discussed in Section 4.2 and Section 4.3.2. [the hydro-climatic regime.](#)

Table 1. Catchments geomorphological and climatic characteristics. Catchments area and average slope are directly calculated in Google Earth Engine. For the slope calculation we use the Shuttle Radar Topography Mission (SRTM) DEM. We obtained elevation and annual precipitation information of the existing dataset directly from published papers (Staudinger et al., 2017; von Freyberg et al., 2018; Ceperley et al., 2020).

355

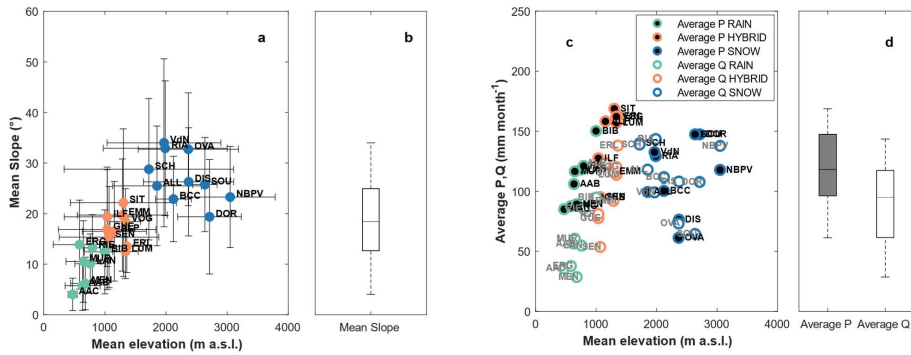


Figure 2 a) Mean slope against mean elevation. Vertical bars represent the mean slope standard deviation, horizontal bars represent min-max elevation range b) boxplot of the mean slope values c) Average precipitation and discharge against elevation d) boxplots of the average precipitation and discharge values. Here and later: boxplots show the quartiles and min-max range. Red crosses indicate the outliers.

360

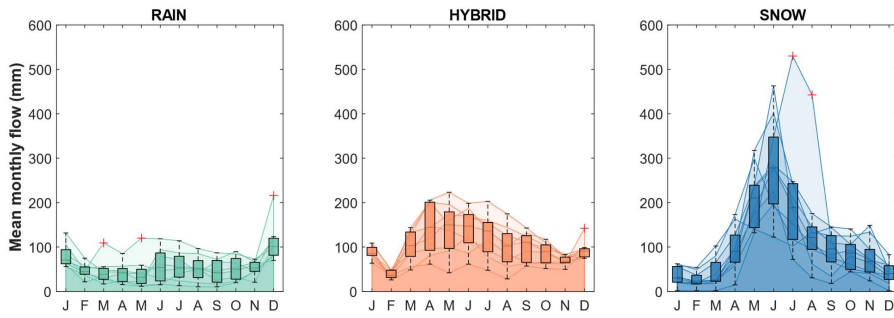


Figure 3 Boxplots of mean monthly flow for all the study catchments grouped according to their flow-regime (rainfall-dominated, hybrid, snow-dominated). Coloured areas represent the monthly flow of each study catchment belonging to the relative regime.

Table 1 Catchments geomorphological and hydro-climatic characteristics. Catchments area and average slope are directly calculated in Google Earth Engine. For the slope calculation we use the Shuttle Radar Topography Mission (SRTM) DEM (Farr et al., 2007). We obtained average elevation and precipitation information of the existing data set directly from published papers (von Freyberg et al., 2018; Ceperley et al., 2020). Discharge (Q), Precipitation (P) and isotopic composition ($\delta^{18}O$) data are all referred to the Period of Sampling (PoS) indicated in this Table. The letter in brackets in the first column indicates the hydro-climatic regime: (R) = Rainfall-dominated, (H) = Hybrid, (S) = Snow-dominated.

ID (Regime)	Area (km ²)	Average Elevation (m a.s.l.)	min Elevation (m a.s.l.)	max Elevation (m a.s.l.)	Average Slope (°)	Dominant geology	Annual Precip. (mm month ⁻¹)	Monthly Q (mm month ⁻¹)	PoS $\delta^{18}O$, Q, P
AAB (R)	46.07	635	519	519-1092	5.73	Sediment. Rock (upper freshwater molasse) Sedimentary Rock	1081.106	56.48	Sep 2010-Feb 2013
AAC (R)	47.25	472	408-560	560	4.02	Unconsolidated sediments (moraine)	1095.85	35.73	Jul 2010-Dec 2011
ALL (S)	28.71	1852	1293-2742	2742	25.48	Sediment. Sedimentary Rock and unconsolidated sediments (flysch, sandstones, profound weathering soils, avalanche debris, hanging rubble and cones of dry rubble)	1651.99	118.04	Sep 2010-May 2015

Celle eliminate

Celle inserite

Celle inserite

Celle eliminate

Celle eliminate

ALP (H)	46.59	1154	<u>845</u>		16.50	Sediment.Sedi mentary Rock and unconsolidated sediments (flysch, conglomerate s, sandstones, marls, carbonate- rich molasse, alluvions)	<u>2112158</u> .2	<u>123.52</u>	<u>May 2010-Dec</u> <u>2015</u>
			<u>845-1894</u>						
BCC (S)	0.14	2121	<u>1932-2515</u>	<u>2515</u>	22.88	Dolomite	<u>1203100</u> .3	<u>111.83</u>	<u>Mar 2010-Oct</u> <u>2017</u>
BIB (R)	31.83	999	<u>827</u>		12.43	Sediment.Sedi mentary Rock and unconsolidated sediments (conglomerat es, sandstones, marls, carbonate- rich molasse, Grindelegg- series, granitic molasse, Forfmoor, alluvions, moraine)	<u>1639150</u> .2	<u>94.78</u>	<u>May 2010-Nov</u> <u>2015</u>
			<u>827-1495</u>						

Celle eliminate

Celle eliminate

Celle eliminate

DIS (S)	42.75	2369	1663- <u>3139</u>	3139	26.28	Metamorphic rock (metagranitoids; amphibolites; mica schist; gneiss; moraine)	139176. <u>4</u>	<u>108.11</u>	<u>Nov 2010-May 2015</u>
DOR (S)	16.99	2711	2390- <u>3430</u>	3430	19.37	Metamorphic rock (gneiss; amphibolites; alluvions)	<u>2164147</u> <u>.4</u>	<u>107.79</u>	<u>Nov 2017-Jan 2022</u>
EMM (H)	124.03	1285	<u>743-2216</u>	743	19.71	Sediment. Rock (mediterranean molasse; subalpine molasse; ground lime formation; calcareous quartz sandstone; moraine; hanging rubble, cone of dry rubble) Sedimentary Rock	1559116 <u>.6</u>	<u>91.99</u>	<u>Jun 2010-Nov 2013</u>

Celle eliminate

Celle eliminate

ERG (R)	260.4 7	584	305	<u>305-1165</u>	13.86	Sediment. Rock (conglomerate, sandstone, subordinately siltstone, marl, crust limestone, oolitic; peloidal and micritic limestone, Staffelegg- formation; Opalinus- Ton, scree) Sedi- mentary Rock	<u>401287.</u> 7	<u>37.88</u>	<u>Jun 2010-Nov</u> <u>2015</u>
ERL (H)	0.74	1359		<u>1117-</u> <u>1650</u>	<u>1650</u> 13.53	Sediment.Sedi- mentary Rock (flysch, eboulis)	<u>2168162.</u> 4	<u>138.04</u>	<u>Jul 2010-May</u> <u>2015</u>
GUE (H)	55.23	1037	<u>556</u>	<u>556-2152</u>	16.84	Sediment.Sedi- mentary Rock and unconsolidated sediments (flysch, eboulis, dry cones, Sequanian, moraine)	<u>124194.</u> 9	<u>77.69</u>	<u>Jul 2010-Dec</u> <u>2012</u>

Celle eliminate

Celle eliminate

ILF (H)	186.94	1037	681	681-2087	19.36	Sediment. Rock (colorful polymietic conglomerate subordinate to sandstone and marl or silty marl; mediterranean molasse; flysch subalpine; alluvions)Sedimentary Rock	1450127.5	81.09	Jul 2010-May 2015
	LAN (R)	59.76		760	598	598-1100	10.08	Sediment. Rock (Napf formation and St.-Gallen formation under thin quaternary cover; Dürrenroth gravel; alluvions)Sedimentary Rock	1195118.2
LUM (H)		1.20	1336	1092-1508	12.49	Sediment.Sedimentary Rock (flysch)	2615157.1	113.63	Oct 2010-Nov 2015

Celle eliminate

MEN (R)	105.0 2	679	447- <u>926</u>	926	6.19	Sediment.Sedi mentary Rock and unconsolidated sediments (variegated sandstone and marl under thin moraine cover, sandstone and marl, moraine)	<u>106089.</u> <u>3</u>	<u>28.64</u>	<u>Jul 2010-Feb</u> <u>2013</u>
MUR (R)	79.92	648	<u>467</u> 467-1036		10.52	Sediment.Sedi mentary Rock and unconsolidated sediments (upper freshwater molasse, moraine, postglacial gravel)	<u>1281116</u> <u>.6</u>	<u>60.57</u>	<u>Jul 2010-Nov</u> <u>2014</u>
NBPV (S)	8.39	3049	2298- <u>3769</u>	<u>3769</u>	23.27	Metamorphic and sediment:sedi mentary rock (phyllites, paragneiss, paraseists)	<u>1413117</u> <u>.8</u>	<u>137.80</u>	<u>May 2013-Sep</u> <u>2015</u>
OVA (S)	26.87	2364	1519- <u>3160</u>	<u>3160</u>	32.73	Dolomite	<u>88761.3</u>	<u>73.21</u>	<u>Aug 2010-Sep</u> <u>2013</u>

Celle eliminate

Celle eliminate

RIA <u>(S)</u>	23.85	1986	<u>881</u>	<u>881-2908</u>	32.93	Metamorphic rock (Biotite, granodiorite, gneiss, mica schist, hanging rubble and cones of dry rubble)	<u>2104129</u> <u>.3</u>	<u>143.49</u>	<u>Jul 2010-Dec 2012</u>
RIE <u>(R)</u>	3.18	794		<u>671-938</u>	13.23	Sediment-Sedimentary Rock and unconsolidated sediments (upper freshwater molasse; moraine)	<u>1555121</u> <u>.1</u>	<u>85.58</u>	<u>Jul 2010-Feb 2013</u>
SCH <u>(S)</u>	107.6 1	1719	<u>487</u>	<u>487-3260</u>	28.78	Sediment-Sedimentary Rock and unconsolidated sediments (flysch; settling mass; rockslide; moraine)	<u>1687140</u> <u>.0</u>	<u>138.93</u>	<u>Apr 2011-May 2015</u>
SEN <u>(H)</u>	350.2 4	1068	<u>554</u>	<u>554-2184</u>	15.35	Sediment-Rock (flysch; sandstone; marls; scists; moraine)Sedimentary Rock	<u>127095</u> <u>2</u>	<u>53.66</u>	<u>Oct 2010-Mar 2013</u>

Celle eliminate

Celle eliminate

Celle eliminate

			768						
SIT (H)	74.23	1301		768-2500	22.15	Sediment. Rock (lower freshwater molasse, Helvetian calcareous limestone, lower Schraffenkalk, moraine)Sedimentary Rock	1870168 .7	115.47	Nov 2010-May 2015
SOU (S)	0.16	2636	2390- 2790	2790	25.74	Metamorphic rock (gneiss)	2164147 .4	64.47	Nov 2017-Jan 2022
VdN (S)	13.55	1966	1189- 3051	3051	34.00	Sediment. Rock (flysch, sandstone, marls)Sedimentary Rock	1591132 .6	99.14	Nov 2015-Dec 2018
VOG (H)	1.57	1335	1038- 1540	1540	18.42	Sediment.Sedimentary Rock (flysch)	2161162 .2	120.24	Jun 2010-Nov 2015

Celle eliminate

370

3 Material and Methods

3.1 Discharge data and catchments boundaries

Daily discharge data for the Erlenbach (ERL), Lümpebach (LÜM) and Vogelbach (VOG) catchments are provided by the Swiss Federal Institute for Forest, Snow and Landscape research (WSL), Birmensdorf, Switzerland. Moreover, streamflow data for the Aabach (AAB) and Guerbe (GUE) catchments are provided by the Office for Waste, Water, Energy and Air (WWEA) of the Canton of Zurich and by the Office for Water and Waste of the Canton of Bern, respectively. Vallon de Nant (VdN) 1-min discharge measurements are obtained via an optical height gauge above the middle point of a trapezoid shape weir (Antoniazza et al., 2022; Michelon et al., 2022), and they are subsequently aggregated to daily streamflow values. Bridge Creek Catchment (BCC) and Noce Bianco at Pian Venezia (NBPV) catchment daily streamflow data are provided by Dr. Giulia Zucco, (University of Padova, Italy). Daily discharge data for the DOR and SOU catchments are obtained aggregating 10-min measurements deriving from piezo-resistive multi-sensors (as described in Section 2). Daily discharge

375

380

data of the remaining 17 Swiss catchments studied by von Freyberg et al. (2018) are provided by the Swiss Federal Office for the Environment (FOEN).

We obtain the .shp of the AAB, GUE, ERL, LÜM and VOG catchments boundaries from the Zenodo data repository reported in Staudinger et al. (2020); the .shp of NBPV, BCC and VdN catchments, are provided by Dr. Giulia Zucco and Dr. Anthony Michelon (University of Lausanne, Switzerland) as personal communication. We delineate the DOR and SOU catchments boundaries in a GIS environment using the 10-m resolution Digital Elevation Model (DEM) available from the Aosta Valley Regional Geoportale. Finally, we obtain the catchment boundaries of the remaining 17 Swiss catchments investigated by von Freyberg et al. (2018) directly from the Swiss Federal Office for the Environment (FOEN).

3.23.1 Young water fraction estimation from seasonal cycles of stable water isotopes in precipitation and streamwater: the “direct” input.

Kirchner (2016a) has demonstrated that the F_{yw} young water fraction can be easily approximated accurately predicted by the amplitude ratios of seasonal sine curves fitted to streamwater stream water and precipitation isotope values. Operatively, seasonal isotope (e.g., $\delta^{18}O$) cycles in streamwater stream water and precipitation can be modelled by:

$$\delta^{18}O_S(t) = A_S \sin(2\pi ft - \varphi_S) + k_S, \quad (1)$$

(2)

$$\delta^{18}O_P(t) = A_P \sin(2\pi ft - \varphi_P) + k_P, \quad (2),$$

(3)

where; $\delta^{18}O$ (‰) is the isotopic composition of water sampled at the time t (expressed in decimal years), A (‰) is the amplitude of the seasonal isotope cycle, φ (in radians) is the phase, f (yr^{-1}) is the frequency and k (‰) is the vertical offset of the seasonal isotope cycle. The subscript “S” refers to streamwater, while the subscript “P” refers to precipitation. As in the work of Kirchner (2016a), we fit the sine curves of Eq. (1) and Eq. (2) on the isotope measurements using the Iteratively Re-weighted Least Squares (IRLS) method (for reducing the influence of outliers) and then estimate the A , φ and k parameters. stream water, while the subscript “P” refers to precipitation. As in the work of von Freyberg et al. (2018), the sine curves of Eq. (2) and Eq. (3) can be fitted on the isotope measurements (using the Iteratively Re-weighted Least Squares method for reducing the influence of outliers), which leads to estimates of A , φ and k parameters. The sine wave is fitted to the isotopes measured in precipitation weighted according to the volume of precipitation to reduce the influence of low-precipitation periods and to account for temporally aggregated rainfall samples (von Freyberg et al., 2018); the sine-fit of stream water isotope measurements can be discharge-weighted or not, using the discharge measured at the moment of sampling as weights (von Freyberg et al., 2018). Consequently, an unweighted amplitude (A_S) or a flow-weighted amplitude (A^*_S) can be obtained. Thus, following Kirchner (2016a), it is possible to calculate the time-weighted or flow-weighted young water fraction fractions (F_{yw} or F^*_{yw}) via the “amplitude ratio approach”:

$$F_{yw} = \frac{A_S}{A_P} \quad (3)$$

$$(4.1)$$

415 We fit a sine wave to the isotopes measured in precipitation according to volume of precipitation to reduce the influence of
low-precipitation periods and to account for temporally aggregated rainfall samples (von Freyberg et al., 2018); the sine-fit
of streamwater isotope measurements can be discharge-weighted or not, using the discharge measured at the moment of
sampling as weights (von Freyberg et al., 2018). Consequently, we obtain an unweighted A_S or a flow-weighted A_S with
which Eq. (3) can be evaluated. The uncertainty of these estimated F_{yw} (flow-weighted or unweighted) are calculated using
420 the Gaussian error propagation (von Freyberg et al., 2018). Flow-weighting was used in both the work of von Freyberg et al.
(2018) and Ceperley et al. (2020). Gallart et al. (2020) highlighted the advantages of the flow-weighted analysis (generally
yielding flow-weighted A_S greater than unweighted A_S) to compensate for subsampled high-flow periods. Thereby, for the
existing dataset, we consider the values of flow-weighted F_{yw} reported in Table 3 of von Freyberg et al. (2018) and in Table
6 of Ceperley et al. (2020) with associated errors.

425 Accordingly, for the additional dataset composed by the DOR and SOU catchments, we apply the procedure above for
calculating the flow-weighted F_{yw} using $\delta^{18}\text{O}$ measurements collected in the period November 2017–January 2022.

3.3 — A new hydro-climatic regime classification: the classifiers

Our analysis focuses on Alpine catchments whose streamflow regimes are dominated by natural precipitation-runoff
transformation processes. The corresponding streamflow regimes are classically divided into those that are rainfall-driven
430 (often called pluvial) and those that are snow-dominated, with or without glacier influence and possibly including hybrid
regimes (Weingartner and Aschwanden, 1992; Moore et al., 2012; Staudinger et al., 2017).

While the streamflow regime terminology is omnipresent in hydrology literature, there is often no formal classification
method provided (Déry et al., 2009). Switzerland has a formal streamflow regime classification into 16 regimes, largely
based on Pardé coefficients (Pardé, 1933), i.e. monthly streamflow ratios (Weingartner and Aschwanden, 1992), used by a
435 few additional authors (Curran and Biles, 2021). Some authors consider mean catchment elevation or human influence
(Piccolroaz et al., 2016). These classifications are typically based on streamflow data and some topographical data (e.g.,
elevation and glacier cover).

We design a new criterion, explained below, for classifying streamflow regimes as rainfall-dominated, hybrid and snow-
dominated, which should be as parsimonious as possible (i.e., using few explicative variables) and account explicitly for the
440 snow cover regime in the catchments. As a proxy for the snow cover regime, we use the average fractional Snow Cover Area
($F_{SC,A}$); we discuss its computation in Section 3.4. Staudinger et al. (2017) classify the catchments in the above-mentioned
clusters grouping some of the regimes defined by Weingartner and Aschwanden (1992) that are built on the streamflow
regime in Switzerland. The tricky points of this “three regimes classification” are the transitions, both from rainfall-

dominated to hybrid catchments and, similarly, from hybrid to snow-dominated ones. Focusing on these transitions, in both cases, we reason that the role of snowpack is crucial. From our knowledge of the regime classification systems already existing in literature, there are no studies that explicitly consider the role of snow. Expansion in satellite data ubiquity, frequency, and accessibility has rendered the assessment of snow cover only recently feasible.

For the classification, we further use a common monthly streamflow ratio, namely the Q_{June}/Q_{DJF} ratio (i.e., ratio of the average flow of June and the sum of average flow of December, January, and February), as a classifier. Flow is relative to catchment area; it is expressed in mm per time step. Using the regime classification of Staudinger et al. (2017) as a base, we compare the monthly streamflow of their catchments belonging to different regimes and we focus thereby on Q_{DJF} (as proxy for winter flow) and Q_{June} (as a proxy for summer flow). It is in fact during these two periods that Q_{June} and Q_{DJF} differ the most between different regime types, as shown in Fig. 2. Accordingly, our new classification scheme (Section 4.2) is based on two variables: the F_{SCA} and Q_{June}/Q_{DJF} ratio.

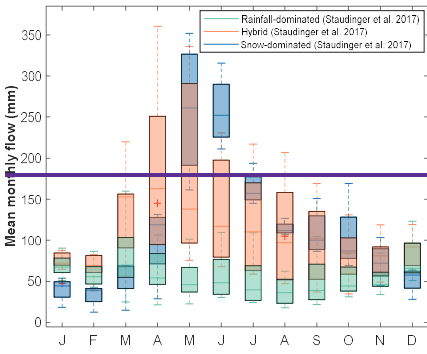


Figure 2. Boxplots of mean monthly flow for catchments studied by Staudinger et al. (2017) and grouped according to their flow regime classification (rainfall-dominated, hybrid, snow-dominated)

3.4 — Average fractional Snow Cover Area (F_{SCA}) computation

The F_{SCA} for each catchment is calculated over the period October 1st 2017– September 30th 2021 (hereafter defined as POI , i.e., Period of Interest) starting from $F_{yw}^* = \frac{A_s^*}{A_p}$.

$$(4.2)$$

Gallart et al. (2020a) highlighted the advantages of the flow-weighted analysis (generally yielding A^*_s greater than A_s) to compensate for subsampled high-flow periods, which would otherwise lead to a young water fraction underestimate. Accordingly, we will consider in this work, for all the study catchments, only the flow-weighted young water fractions. The uncertainty of these estimated F^*_{yw} can be obtained using a Gaussian error propagation (von Freyberg et al., 2018).

The analytical choice of using the amplitude (A_P) fitted on precipitation isotopes, instead of the amplitude ($A_{P_{eq}}$) fitted on the equivalent precipitation (i.e., rain + snowmelt) isotopes, for estimating F_{yw}^* implies that the snowpack is considered as part of the catchment storage and that the damped seasonal cycle observed in the stream is given by the mixing of precipitation with snowpack and subsurface storage (the last two considered as a single entity), as illustrated in Fig. 4:

470

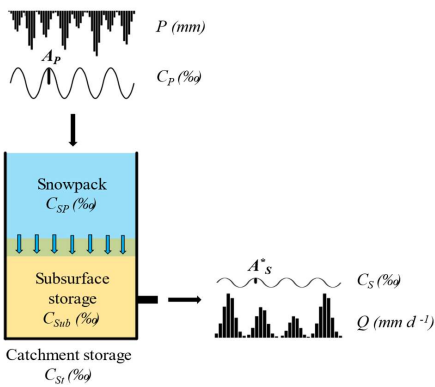


Figure 4 Schematic representation of the “direct input” approach for estimating F_{yw}^* . Light blue arrows indicate that meltwater coming from the snowpack preferentially infiltrates. The term “C” refers to the isotopic composition. The subscripts: “P” refers to “Precipitation”, “S” refers to “Stream”, “SP” refers to “Snowpack”, “Sub” refers to “Subsurface storage” and “St” refers to “Catchment storage”.

475

For the published data sets (von Freyberg et al., 2018; Ceperley et al., 2020), we consider the F_{yw}^* values, with associated errors, published or provided by the authors, while for the DOR and SOU catchments we estimate F_{yw}^* applying the methodology described in this Section (more info are available in the Supplementary Material). A plot of F_{yw}^* against mean elevation for the 27 study sites is shown in Fig. 5. F_{yw}^* values for all the study catchments are reported in Table 2.

480

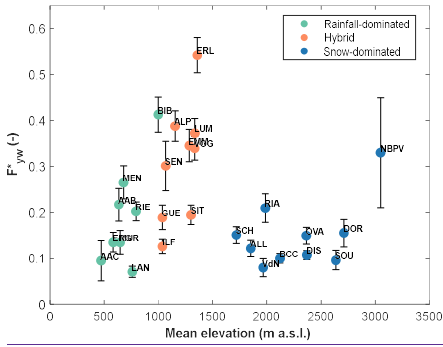


Figure 5 F_{yw}^* as function of mean catchment elevation.

3.2 Snow cover persistence quantified through the average fractional snow cover area (F_{SCA})

485 In this paper, we quantify the snowpack persistence calculating the average fractional Snow Cover Area (F_{SCA}). It is
 490 calculated, for each catchment, over the period October 1st, 2017- September 30th, 2021 (hereafter defined as PoC, i.e.,
 period of calculation) using Sentinel-2 L2A satellite images. Temporally, this relatively recent satellite has increased the
 visitation frequency to more than a sub-weekly temporal resolution and increased the spatial resolution to 20 m for snow
 cover (Gascoin et al., 2019). High temporal resolution makes Sentinel-2 images preferable to Landsat images, which are
 495 available only once every 16 days and whose total number is often further reduced because of cloudiness (Hofmeister et al.,
 2022). The PoC generally differs from the PoS for the 27 study catchments. This is because Sentinel-2 L2A satellite images
 are not available before March 2017. For each image available in the PoC , we calculate the Normalized-Difference Snow
 Index (NDSI) as suggested in the work of Dozier (1989):

$$NDSI = \frac{r_{green} - r_{SWIR}}{r_{green} + r_{SWIR}} \quad (4)$$

495
$$NDSI = \frac{r_{green} - r_{SWIR}}{r_{green} + r_{SWIR}} \quad (5)$$

where r_{green} is the reflectance in the green band (Sentinel-2 band 3) and r_{SWIR} is the shortwave infrared reflectance band
 (Sentinel-2 band 11). We classify as snowy pixels those with a NDSI value > 0.4 (Dozier, 1989). Based on the pixel-wise
 snow classification, we compute f_{SCA} as in the works of Di Marco et al. (2020) and Hofmeister et al. Based on the pixel-wise
 snow classification, we compute the snapshot fractional Snow Cover Area (f_{SCA}) as in the works of Di Marco et al. (2020)
 500 and Hofmeister et al. (2022):

$$f_{SCA} = \frac{N_{snow}}{N_{tot} - N_{clouds}}, \quad (5)$$

(6)

where N_{snow} is the number of snow cover pixels according to the applied NDSI threshold method, N_{tot} is the total number of pixels within the catchment area and N_{clouds} is the number of pixels classified as clouds and water bodies (Hofmeister et al., 2022). We identify the cloudy pixels directly using the Sentinel-2 band “Scene Classification Map”. We

operatively calculate N_{snow} , N_{tot} and N_{clouds} using a Google Earth Engine script. We identify the cloudy pixels directly using the Sentinel-2 band “Scene Classification Map”. We operatively calculate N_{snow} , N_{tot} and N_{clouds} using a Google Earth Engine (Gorelick et al., 2017) script.

Using this procedure for calculating f_{SCA} , we sometimes obtain $f_{SCA} > 1$, typically for winter satellite images. The NDSI threshold method is generally able to distinguish between snow and no-snow pixels (Aalstad et al., 2020). Accordingly, clouds and snow have similar reflectance in the green band, but clouds highly reflect in the shortwave infrared band, while snow reflectance is low in this band. Thus, the N_{snow} estimation is generally accurate. On the other hand, it is necessary to

reduce not consider the number of false positive pixels deriving from clouds detection (i.e., snow classified as clouds).

During winter if $f_{SCA} > 1$, we calculate f_{SCA} as N_{snow} / N_{tot} since this is likely the only heuristic solution that N_{snow} approaches very close to N_{tot} . Accordingly, it is easy to have $N_{tot} - N_{clouds} < N_{snow}$ if N_{clouds} incorporate pixels that are in fact snow covered. In these cases, we assume that $N_{clouds} = N_{tot} - N_{snow}$ (i.e., $f_{SCA} = 1$) guarantees no overestimation. Moreover, by looking at sample Sentinel-2 images during the summer periods for all the catchments, we impose $f_{SCA} = 0$ during July and August, since when f_{SCA} other than 0 has, this usually results from falsely identified clouds as snow; imposing $f_{SCA} = 0$ clearly leads to fewer errors (missed occasional summer snowfall events of very shallow depth) than falsely accounting for (far more) frequent clouds. The Noce Bianco Pian Venezia (NBPV) catchment is an exception: we do not impose $f_{SCA} = 0$ during July and August since it generally has snow over the glacier also during summer. Finally, we remove small inaccuracies by applying a moving compute the average on a window of three fractional snow cover area (F_{SCA}) for each catchment by averaging all f_{SCA} values available for all snow images over the f_{SCA} timeseries in the PoC, without interpolation between the time steps.

After this filtering step, we compute the average f_{SCA} (i.e., F_{SCA}) for each catchment by averaging all f_{SCA} values available for all snow images in the PoC, without interpolation between the time steps.

3.5 Accounting for groundwater: fraction of quaternary deposits (F_{qd}), Winter Flow Index (WFI) and baseflow fraction (F_b)

3.3 Some authors have revealed the key possibility of unconsolidated sediments (e.g., talus, moraine, alluvium) storing groundwater in Alpine catchments (Christensen et al., 2020; Hayashi, 2020; Arnoux et al., 2021). Fraction of Quaternary deposits, low-flow duration and the groundwater contribution to the stream

We use the same Winter Flow Index (WFI) as Arnoux et al. (2021), as indicated by Eq. 7:

$$WFI = \frac{Q_{NM7}}{Q_{mean}} \quad (7)$$

The stored water in these deposits can in fact sustain streamflow during the low-flow period (Hayashi, 2020; Arnoux et al., 2021), i.e. during long periods without direct water input, especially during winter, which can last 6 months or more in high elevation catchments. Such sustained flow during long periods points towards important amounts of stored water that is well connected to the streamflow network and thereby remains accessible throughout the low flow period and also during glacier and snowpack recession due to climate change (Somers et al., 2019). It is thus natural to think that groundwater might also play a key role in driving F_{3w} in Alpine catchments.

We describe in this section how to calculate three quantities that are all, directly or indirectly, linked to groundwater: fraction of quaternary deposits (F_{qd}), the Winter Flow Index (WFI) and baseflow fraction (F_{bf}). First, we estimate the proportion of quaternary deposits similarly to Arnoux et al. (2021). Operatively, for the 23 Swiss catchments of our dataset, we calculate the portion of the catchment area occupied by quaternary deposits using the Geological Atlas of Switzerland (GeoCover dataset, 1:25000 scale) freely available from the *Federal Office of Topography swisstopo*. We use the geological sheets that intersect the catchments boundaries for evaluating the portion of unconsolidated sediments area (A_{qd}) covering the catchments area (A). Thus, we calculate the fraction of quaternary deposits (F_{qd}) as:

$$F_{qd} = \frac{A_{qd}}{A} \quad (6)$$

We repeated the same procedure for the DOR and SOU catchments by using the regional geological map for obtaining this fraction. For the DOR and SOU catchments the vectorized Valsavaranche geological map (1:100000 scale) is provided by the *Cartography Office of SCT Geoportal*. For the NBPV and BCC catchments the *shp* of unconsolidated sediments is provided by Dr. Giulia Zucco, where Q_{NM7} is the minimum discharge over seven consecutive days during the winter period (from November to June) and Q_{mean} is the mean annual discharge. We calculate it for the 27 study catchments during the PoS. Similarly to Arnoux et al. (2021), we calculate the portion of the catchment area occupied by Quaternary deposits (A_{qd}) (available from National or Regional geological data set) with respect to the total catchment area (A). Thus, we calculate the fraction of Quaternary deposits (F_{qd}) as reported by Eq. 8:

$F_{qd} = \frac{A_{qd}}{A}$. The spatial cover of quaternary deposits for the 27 study catchments is reported in Fig. 1.

To complement geological information, we also calculate the Winter Flow Index (WFI), a low-flow indicator that is generally used to evaluate the potential of catchments to store groundwater (Paznekas and Hayashi, 2016; Cochand et al., 2019; Hayashi, 2020; Arnoux et al., 2021):

$$WFI = \frac{Q_{NM7}}{Q_{mean}} \quad (7)$$

where Q_{NM7} is the minimum discharge over seven consecutive days during the winter period (from November to June) and Q_{mean} is the mean annual discharge (Arnoux et al., 2021).

Finally, we estimate the baseflow contribution to streamflow that is generally assimilated to the flow from groundwater and, accordingly, is associated to groundwater processes (Hall, 1968; Duncan, 2019). Additionally, Duncan (2019) provides a

specific technique that allows estimation of separate components with physical relevance in the case that baseflow separation techniques were not applied to describe physical processes. We apply the

(8)

The area covered by such deposits for a sample area of our study region is reported in Fig. 6.

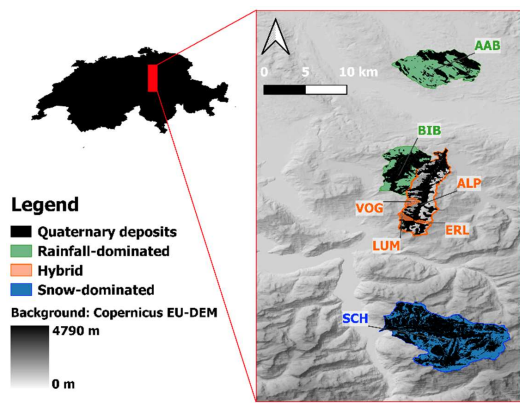


Figure 6 Proportion of quaternary deposits (black colour) covering the area of seven study catchments in Switzerland.

To relate WFI to low flow, we apply the recent baseflow separation technique described by Duncan (2019) to the discharge time series of the 27 study catchments. Specifically, we apply it to the available discharge measurements within the temporal windows of streamwater isotope sampling. For the 22 Swiss catchments from von Freyberg et al. (2018), we consider the sampling period reported in Table 1 of their published paper. For VdN, NBPV and BCC catchments we consider the time windows November 2015–December 2018, May 2013–September 2015, March 2010–October 2017, respectively. Finally, for the DOR and SOU catchments, we consider discharge measurements in the period November 2017–January 2022. To express the groundwater contribution to streamflow in a form that is directly comparable with the young water fraction, we define the baseflow fraction (F_b) as: (within the PoS indicated in Table 1). In short, this method comprises a single backward pass through the data to fit an exponential master baseflow recession curve (Eq. 9.1), followed by a single forward pass (Eq. 9.2, Eq. 9.3) of the Lyne and Hollick (1979) algorithm to smooth the connection between segments of the master recession, simulating a gradual groundwater recharge during the runoff event (Duncan, 2019):

$$M(t_{i-1}) = \frac{M(t_i) - c}{k} + c \quad (9.1)$$

$$Q_q(t_i) = kQ_q(t_{i-1}) + (M(t_i) - M(t_{i-1})) \frac{1+k}{2} \quad (9.2)$$

$$585 \quad Q_{bf}(t_i) = M(t_i) - Q_q(t_i) \quad (9.3)$$

where $M(t_i)$, $Q_q(t_i)$ and $Q_{bf}(t_i)$ are the master recession value, the quick recession flow and the baseflow at time t_i , respectively. In this study, we consider daily time steps (i.e., $t_i - t_{i-1} = 1$ day). This method has 2 parameters: k is the recession constant; c is a constant flow added to the exponential decay component. We set the recession constant $k = 0.925$ (Nathan and McMahon, 1990); we add no constant flow to the exponential decay (i.e., in terms of Duncan (2019) method, $c=0$). A Matlab © code with the implementation of the Duncan (2019) baseflow filter has been made available in the Supplementary Material.

590

To express the catchment storage contribution to streamflow in a form that is directly comparable to the young water fraction, we define the baseflow fraction (F_{bf}) as reported in Eq. 10:

$$F_{bf} = \frac{1}{n} \sum_{i=1}^n \frac{Q_{bf}(t_i)}{Q(t_i)} \quad (10)$$

595 where $Q_{bf}(t_i)$ is the baseflow (mm d^{-1}) at the time t_i (obtained as indicated by Eq. 9.3) and $Q(t_i)$ is the discharge (mm d^{-1}) at the time t_i . Following the 0.9 to 0.95 range recommendation for k of Nathan and McMahon (1990), we test the uncertainty of this value by drawing random samples (10000 values) from a normal distribution with mean 0.925 and standard deviation 25% of the range given by Nathan and McMahon (1990) (i.e. standard deviation of 0.0125 which ensures that the 10% and 90% sample percentiles correspond to the original range). Thereby we obtain 10000 values of F_{bf} for each catchment, of which we compute the standard deviation.

600 As introduced in Section 1, F_{yw}^* can be low if the snapshot young water fraction $F_{yw}(t_i)$ is very low for many time steps. Past studies revealed that F_{yw}^* increases with the catchment wetness (von Freyberg et al., 2018; Wilusz et al., 2017). If we consider the discharge (Q) as a proxy for the catchment wetness, we can reliably assert that $F(t_i)$ is low for low $Q(t_i)$. Thus, another important variable is the duration of the low-flow period. In this study, we define a low-flow period (T_{Low}) as follows:

$$605 \quad T_{Low} = \forall t_i : \frac{Q_{bf}(t_i)}{Q(t_i)} \geq 0.85 \quad (11)$$

Thus, a low-flow period is defined here as a period when 85% of the total flow is composed of baseflow (i.e., baseflow-dominated). Accordingly, we define the low-flow duration (LFD), as the proportion of the time-steps (e.g., days) in the PoS that can be considered as a low flow period according to Eq. (11).

610 **4 Results and Discussion – Towards a harmonious and exhaustive framework of the hydrological processes that drive the young water fraction variations with elevation.**

We present and discuss hereafter (Section 4.1, 4.2, 4.3 and 4.4) the identified relations between F_{yw}^* and the studied explanatory variables (F_{gd} , F_{bf} , LFD and F_{SCA}), followed by the emerging perceptual model that describes the main processes driving the F_{yw}^* variations with mean catchment elevation and harmonizes our results with previous studies (Section 4.5).

615 **4.1 The role of Quaternary deposits**

Confirming the results of Arnoux et al. (2021), we find a negative statistically significant correlation between F_{yw}^* and WFI ($\rho_{\text{Spearman}} = -0.4$, p-value = 0.04, see Fig. S5), suggesting (unsurprisingly) that more groundwater contribution to streamflow increases the water age. WFI and F_{gd} values for all the study catchments are reported in Table 2. To analyze the relationship of F_{yw}^* with Quaternary deposits we rule out the SOU and BCC catchments since they show $F_{gd} = 0$ (see Table 2). Including catchments with $F_{gd} = 0$ would bias the analysis since something that is absent cannot have a role in modulating the share of groundwater and thus the young water fraction in the stream.

620 Focusing first only on the snow-dominated catchments, a linear fit on the data returns a negative slope of -0.31 ($R^2 = 0.4$), indicating a reduction of F_{yw}^* with increasing F_{gd} (Fig. 7a). Moreover, we find a Spearman rank correlation coefficient of -0.62 with a p-value of 0.12, meaning a negative, but not statistically significant correlation between F_{yw}^* and F_{gd} . This result can be explained by considering several factors. First, water storage in Quaternary deposits is not the only groundwater storage contribution to the stream in such environments: additional storage is provided by the bedrock fractures (Gleeson et al., 2014; Jasechko et al., 2016; Martin et al., 2021), possibly caused by rock stress and high erosion rates and by the bedrock geology, which has influence on groundwater retention capacity (Hayashi, 2020). Second, the area covered by Quaternary deposits could be a not sufficient good proxy of the groundwater storage potential: the knowledge of the thickness of these deposits (i.e., their volume) and the bedrock topography are crucial factors for controlling groundwater storage (Arnoux et al., 2021; Hayashi, 2020) but corresponding data is not available to date.

635 F_{yw}^* values of the hybrid catchments reveal a weak positive correlation with Quaternary deposits ($\rho_{\text{Spearman}} = 0.1$, p-value = 0.81) while, for rainfall-dominated catchments, they show a negative correlation ($\rho_{\text{Spearman}} = -0.5$, p-value = 0.22); however, both correlations are not statistically significant. These weak correlations suggest that F_{gd} represents only a limited part of the catchment geology responsible for groundwater flow and that it can only be considered as a first-order measure of geological groundwater storage.

We furthermore observe that F_{gd} decreases with mean catchment elevation in our data set (Fig. 7b), revealing a negative statistically significant correlation ($\rho_{\text{Spearman}} = -0.5$, p-value < 0.01). This negative correlation reflects the fact that F_{gd} decreases when the mean slope increases (Arnoux et al., 2021).

640 To conclude, we stress that more catchments and more geological information would be required to statistically validate these observations about the role of the groundwater storage potential for explaining young water fraction variations.

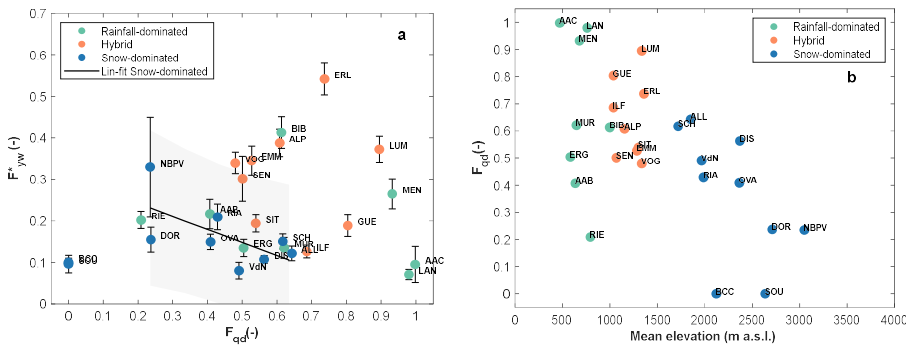


Figure 7 a) Young water fraction against fraction of Quaternary deposits b) Fraction of quaternary deposits against mean catchments elevation

4.2 Stored (old) water contribution to streamflow (F_b) and F_{yw}^*

The baseflow time series resulting from the baseflow separation of Duncan (2019) for six representative study catchments (two of each regime) are reported in Fig. 8 (complete results in Fig. S2). This figure shows the effect of groundwater recharge from rain and snowmelt through the “smoothed” baseflow proposed by Duncan (2019). This “smoothing” simulates a delayed storage contribution to the stream following the recharge phase during an input event. This recharge phase promotes the system wetness, thus favoring an increasing quick flow. The increasing quick flow during events also leads to an increase of $F_{yw}(t)$, as found by previous works (von Freyberg et al., 2018). However, the relative amount of baseflow remains high during events: the average baseflow fraction during the high-flow period is 0.49 and 0.52 for hybrid and rainfall-dominated catchments, while it is 0.63 for snow-dominated catchments. In agreement with worldwide stable-isotope-based hydrograph separations results (Jasechko, 2019), this outcome underlines the mobilization of stored water (i.e., old water) during rainfall and snowmelt events, and this process seems to be particularly relevant in high-elevation catchments. Accordingly, in snow-dominated systems, the snowmelt largely transits through the groundwater store (Hayashi, 2020; Cochand et al., 2019; Du et al., 2019; Flerchinger et al., 1992; Martinec, 1975), as schematized in Fig. 4, and the very high baseflow in high mountain catchments during summer is a direct sign of meltwater infiltration and percolation to groundwater that pushes old snowmelt (the main groundwater storage component) out to the stream network, as also found by Martinec (1975). This is also supported by the fact that groundwater, in such catchments, often has the isotopic signature of snowmelt (Michelon et al., 2022; Pavlovskii et al., 2018).

Looking at the overall flow (and not only at the high-flow periods), F_{bf} is generally lower for hybrid catchments (average $F_{bf} = 0.67$) than for rainfall-dominated (average $F_{bf} = 0.74$) and snow-dominated catchments (average $F_{bf} = 0.83$). In the BCC catchment, we find a F_{bf} (0.87) that is consistent with previous findings of Penna et al. (2016) using stable water isotopes: they have shown that, on average, from 80% to 98% of BCC discharge is composed of pre-event water (assumed to represent groundwater). The values of F_{bf} for all the study sites are reported in Table 2. On average, the F_{bf} computed over the entire PoS are higher than those computed during the high-flow periods. This result suggests, unsurprisingly, that the largest amount of stored water is released during low-flow periods. Accordingly, the variations of F_{bf} with elevation among different catchments (Fig. 9b) can be explained considering the changes in low-flow duration (LFD) with elevation, as will be discussed in Section 4.3.

Baseflow filters were already applied in previous studies and their results were correlated with F_{yw}^* . For example, von Freyberg et al. (2018) found a strong positive correlation ($\rho_{\text{Spearman}} = 0.73$, p-value < 0.001) between F_{yw}^* and the Quick-flow Index (QFI), calculated as the average ratio between $(Q - Q_{bf})$ and Q , where Q is the daily discharge and Q_{bf} is the daily baseflow calculated in their paper with the Lyne and Hollick (1979) baseflow filter. Relating the F_{bf} to F_{yw}^* , we have found a strong negative correlation ($\rho_{\text{Spearman}} = -0.75$, p-value < 0.001), showed in Fig. 9a, consistent with previous results of von Freyberg et al. (2018).

In snow-free systems, F_{yw}^* is by definition related to F_{bf} . Baseflow is composed of groundwater and groundwater is the dominant source of old water in such systems (in absence of large lakes). In snow-influenced systems, through the “direct input” approach for estimating F_{yw}^* , we consider the snowpack (i.e., a temporarily old water storage) as part of the catchment storage. However, the share of snowmelt (with age > 3 months) that flows off quickly as surface or fast subsurface runoff will not show up in F_{bf} . In other words, F_{bf} is not able to take into account all the snowmelt, but only the part of meltwater that infiltrates and recharges the groundwater storage, which is a large portion of the overall snowmelt.

4.2.1 The complementarity between the fraction of baseflow (F_{bf}) and the young water fraction (F_{yw}^*)

A by-product of this work is that the estimated F_{bf} , applying the Duncan (2019) baseflow filter, is roughly the complementary term of F_{yw}^* (Fig. 9a, Fig 9b) which is an important result for catchments where isotope measurements are missing. In such catchments, F_{yw}^* could potentially be estimated without the application of the amplitude ratio approach as:

$$F_{yw}^* \simeq 1 - F_{bf} \quad (12)$$

Some of our case studies show considerable “residuals” of $1 - (F_{bf} + F_{yw}^*)$ (Fig. 9b). This is partially due to the uncertainty of the parameters used for estimating F_{bf} . In this regard, Duncan (2019) suggests some calibration guidelines to obtain an optimal parameters set for baseflow estimation per catchment. In this work, we did not use the calibration guidelines, but we simply used the recession parameter proposed by Nathan and McMahon (1990) in order to achieve factual and reproducible results. In addition, the estimation of baseflow during an event is generally less rigorous than during the recession phase (Duncan, 2019), affecting the F_{bf} estimation. Moreover, F_{yw}^* values are influenced by the sampling rate: the higher is the

frequency of sampling, the higher is the young water fraction (Gallart et al., 2020a; Stockinger et al., 2016). Thus, the young water fraction calculated with the “amplitude ratio” approach generally underestimates the “real” young water fraction, and we simply compensate by computing the flow-weighted young water fraction (F_{yw}^*). In hybrid and snow-dominated catchments these “residuals” can also be explained considering that the F_{yw} does not include surface runoff or fast lateral subsurface flow of meltwater, likely older than 2-3 months, following a snowmelt event. On the other hand, these residuals might also be related to the non-linear recession behavior of catchments, which was shown by Santos et al. (2018) to be dominant for Swiss low elevation (i.e., rain-dominated) catchments, in which case the exponential recession assumption of the baseflow filter necessarily leads to less reliable results (Duncan, 2019).

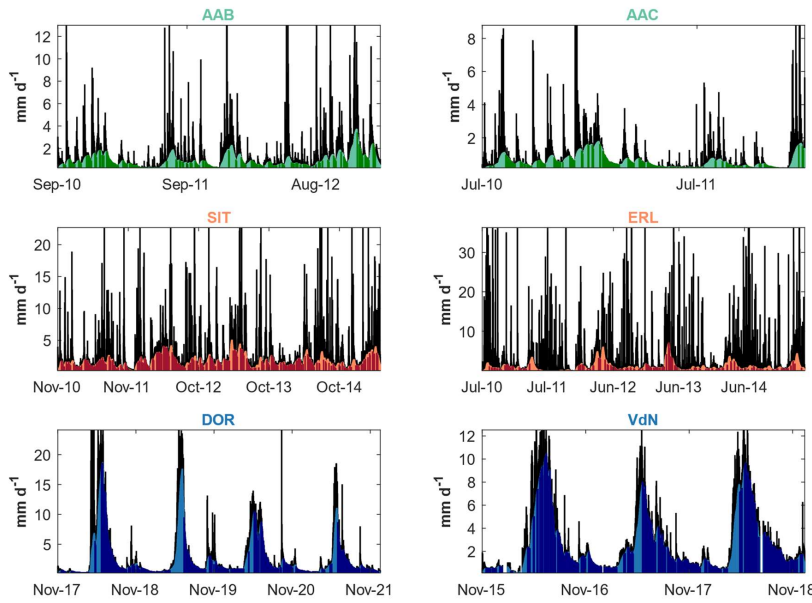


Figure 8: Baseflow separation for six representative study catchments using the Duncan (2019) filter. The black area represents the daily discharge, while the coloured area represents the estimated daily baseflow, where Q_{bf} is the amount of daily baseflow (mm d^{-1}) we obtain using the baseflow separation technique described in the work of Duncan (2019), Q is the daily discharge (mm d^{-1}), t_i is the time step for which we have discharge measurements (where the subscript “i” refers to a specific day) and n is the total number of days within the considered time window.

710 **4—Results**

4.1—Young water fraction estimation for DOR and SOU catchments

We apply the methodology described in Section 3.2 to estimate the young water fraction in DOR and SOU catchments. The unweighted F_{yw} values are equal to 0.1 ± 0.02 for both DOR and SOU catchments. In contrast, the flow-weighted F_{yw} are 0.16 ± 0.03 and 0.01 ± 0.02 for DOR and SOU catchments, respectively. Thus, we find a 60% increase of the flow-weighted F_{yw} for the main catchment, while flow-weighted F_{yw} remains unchanged for the very small lateral subcatchment. The F_{yw} results for these two high-elevation catchments agree with F_{yw} estimated by Jasechko et al. (2016), Lutz et al. (2018), Ceperley et al. (2020), who found less young streamflow in mountains than in other landscapes.

4.2—The new hydro-climatic regime classification

Two selected variables, Q_{June}/Q_{DJF} and F_{SCA} , classify catchments into three classes using our streamlined methodology: rainfall dominated, hybrid and snow dominated; these have the same names as the ones proposed by Staudinger et al. (2017) but the classification is not based on the same criteria.

In order to achieve a classification as consistent as possible with that of Staudinger et al. (2017), but based on these two variables, we propose the thresholds presented in Table 2:

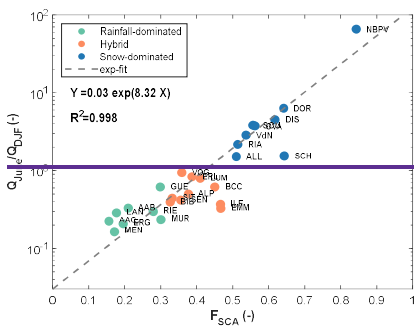
725 **Table 2. New formal classification scheme for defining the catchments hydro-climatic regime using two variables: the F_{SCA} and Q_{June}/Q_{DJF} ratio.**

Condition 1	logical	Condition 2	Hydro-climatic regime
$Q_{June}/Q_{DJF} \leq 1$	&	$F_{SCA} < 0.3$	Rainfall-dominated
$Q_{June}/Q_{DJF} \leq 1$	&	$0.3 \leq F_{SCA} \leq 0.5$	Hybrid
$Q_{June}/Q_{DJF} > 1$	&	$F_{SCA} \geq 0.5$	Snow-dominated

The catchment's hydro-climatic regimes defined with these thresholds for the two variables or classifiers are generally consistent with those of Staudinger et al. (2017) (Table S1). The only exceptions are the BIB and GUE catchments whose regimes switch from rainfall-dominated to hybrid (BIB) and vice-versa (GUE). The hydro-climatic regime switch arises for these two catchments because their Q_{June}/Q_{DJF} ratio are < 1 , while their F_{SCA} (0.32 for BIB and 0.29 for GUE) are very close to our selected threshold of 0.3. Following our classification scheme, the 27 study catchments are equally distributed over the three classes: 8 rainfall-dominated catchments, 10 hybrid catchments and 9 snow-dominated catchments. The regime of each catchment is reported in Table S1.

735 The two selected classifiers are positively correlated ($\rho_{\text{Spearman}} = 0.89$ p -value < 0.01). Moreover, fitting an exponential model ($a \cdot e^{bF_{SCA}}$) on the Q_{June}/Q_{DJF} vs F_{SCA} points, we obtain $a = 0.03$ (confidence bounds: $0.02 \div 0.04$) and $b = 8.32$ (confidence bounds: $7.95 \div 8.70$) with a very high $R^2 = 0.99$ (Fig. 3, the 95% confidence bounds of the coefficients are obtained through a robust fit using the bisquare weighting function in Matlab R2019b). This result suggests that the easy-to-calculate

Q_{June}/Q_{DJF} ratio is a good predictor of the snow regime, here represented by F_{SCA} . Thus, if F_{SCA} data are missing, it is possible to use the exponential relationship (Fig. 3) for a first order estimate of the second classifier. Some catchments, specifically SCH, ILF and EMM fall away from the curve. They are hybrid or snow-dominated catchments with large areas ($>100 \text{ km}^2$) and wide elevation ranges ($>1400 \text{ m}$). In such cases the summer flow is more influenced by summer rainfall at lower elevations and snowmelt preferentially occurs during spring, reducing the Q_{June}/Q_{DJF} ratio. For catchments with these characteristics, the use of the exponential relationship underestimates the F_{SCA} .

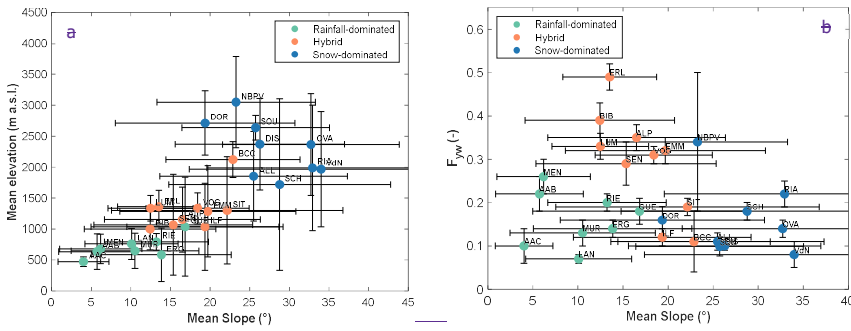


745 **Figure 3.** Scatterplot of the 2 selected classifiers: Q_{June}/Q_{DJF} and F_{SCA} . It shows the strong correlation between the two classifiers.

4.3 — New explanatory variables for the F_{yw} elevation gradients

Initial evidence of low F_{yw} in high elevation catchments is given in the work of Jasechko et al. (2016). Based on the analysis of 254 worldwide watersheds, their work reveals a reduction of F_{yw} in steeper terrains. A first physical explanation of this result could be related to deep vertical infiltration caused by fractures generated by the high stress that rocks have to endure in complex terrain morphologies such as those of high elevation environments (Gleeson et al., 2014; Jasechko et al., 2016). Moreover, the higher the topographic roughness is, the longer are the flow paths, with a consequent rise of transit time (Gleeson and Manning, 2008; Frisbee et al., 2011; Jasechko et al., 2016).

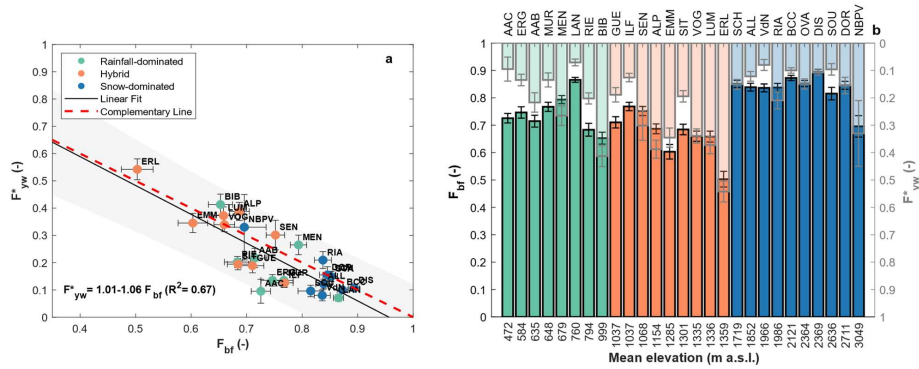
750 Our dataset is characterized by a general increase of slope with elevation (Fig. 4a). Despite this, we do not find significant correlation between F_{yw} and mean slope ($\rho_{\text{Spearman}} = -0.25$, p-value = 0.22) (Fig. 4b). The correlation becomes significant only when the rainfall-dominated catchments are removed from the analysis ($\rho_{\text{Spearman}} = -0.7$ p-value < 0.01). This result suggests that there is an increasing rate of infiltration when the hydro-climatic regime transitions from hybrid to snow-dominated. We probed deeper into the role of snow and groundwater in lowering the F_{yw} to understand the hydrological function of these focus catchments.



760 **Figure 4** a) Catchments plotted according to mean elevation and mean slope. The vertical bars correspond to the elevation range (i.e., max elevation minus minimum elevation). The horizontal bars correspond to \pm standard deviation b) Young water fractions against mean slope. The horizontal and vertical bars correspond to the uncertainty range (\pm standard deviation) given in the original sources or calculated here for DOR and SOU catchments.

4.3.1 — Fractional Snow Cover Area (f_{SCA}) and F_{yw}

765 **The darker colour represents a time step in which at least the 85% of the daily discharge is composed by baseflow.**



770 **Figure 9** a) Young water fraction plotted against fraction of baseflow; vertical and horizontal bars represent \pm standard deviation. Grey area represents the 95% prediction bounds of a linear regression of F_{yw}^* on F_{br} b) Fraction of baseflow and young

water fraction against mean elevation. Bars with black edge indicate F_{bf} (left axis), while bars with grey edge indicate F_{yw}^* (right axis). Vertical bars represent +/- standard deviation.

4.3 Low-flow duration (LFD) and F_{yw}^*

775 The values of LFD for all the study sites are reported in Table 2. Specifically, LFD is lower for hybrid catchments (median
LFD = 0.39), and it is increasingly higher for rainfall (median LFD = 0.50) and snow-dominated catchments (median LFD =
0.62). In hybrid catchments, the presence of rain and snowmelt events during large parts of the year and the relatively low
(compared to rainfall-dominated catchments) evapotranspiration due to reduced temperatures (Goulden et al., 2012), strongly
reduces the duration of low-flow periods, and this is also visible from the recurring discharge peaks (Fig. 8.) In low-lying,
780 rain-dominated catchments, evapotranspiration and precipitation are respectively higher and lower than in hybrid
catchments, leading to longer low-flow periods (usually during summer and autumn). Under current climate and according to
our data set, in snow-dominated catchments we observe longer winter low-flow periods (streamflow decreasing below 0.5
to 1 mm/d for the highest locations, see Fig. S6) on an annual scale than in hybrid catchments. To gain additional insights into
the high LFD in snow-dominated catchments and the low LFD in hybrid catchments, it is necessary to further consider the
785 role of snowpack persistence, discussed in the following Section. The variations of LFD with elevation are shown in Fig.
11b.

It is well known that low-flow periods are typically baseflow-dominated (or old water dominated). Accordingly, as
anticipated in Section 4.2, the variation of F_{bf} between catchments reflects the proportion of the low-flow duration during the
PoS. We observe that the higher the LFD is, the higher is the F_{bf} ; in fact, they are strongly positively correlated ($\rho_{\text{Spearman}} =$
790 0.97, p-value < 0.001) as shown in Fig. 10. The negative correlation between LFD and F_{yw}^* is lower ($\rho_{\text{Spearman}} = -0.75$, p-
value < 0.001, Fig. 11a) but nevertheless suggests that LFD is an important predictor for F_{yw}^* .

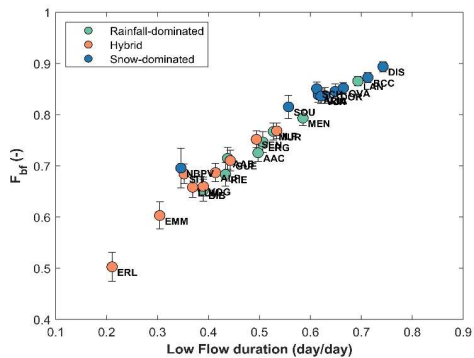


Figure 10 F_{bf}^* against the low Flow Duration (LFD)

795

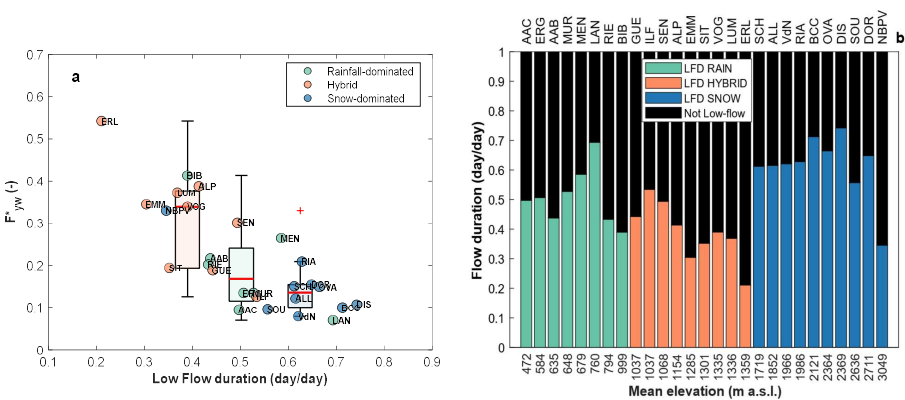


Figure 11 a) F^*_{yr} against the Low Flow Duration, LFD. Boxplots of F^*_{yr} for catchments belonging to the same regime are plotted in correspondence to the median LFD. b) LFD against mean elevation.

4.4 The role of snowpack persistence

800

We next explore the presence of an ephemeral or seasonal snowpack as a relevant factor for the time-concentration of liquid water input and for LFD. We consider the $F_{SC,t}$, calculated as reported in Section 3.2, as a proxy of the snowpack persistence. The $F_{SC,t}$ values for all the study sites are reported in Table 2. The underlying $f_{SC,t}$ timeseries for six representative study

catchments (two for each hydro-climatic regime) are reported in Fig. 5, whereas the timeseries for all the study sites are available in Fig. S2 (complete results in the Supplementary Material (Fig. S2)).

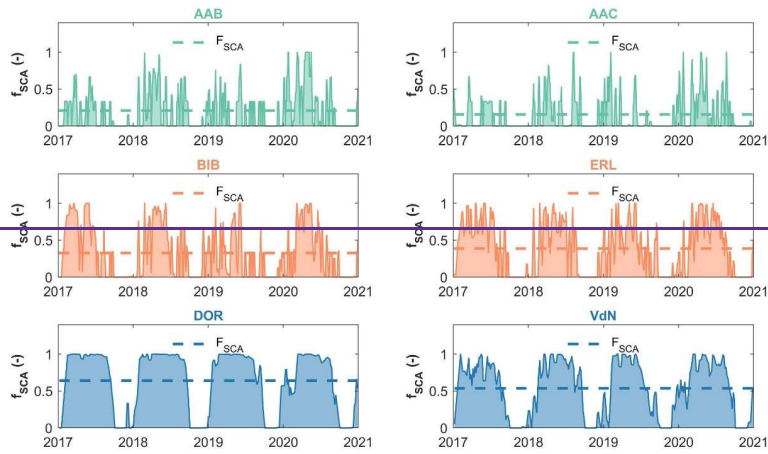


Figure 5. Timeseries of f_{SCA} for 6 representative study sites. All the catchments (two for each hydro-climatic regime), illustrating the gradual increase of the F_{SCA} passing from rainfall-dominated to snow-dominated catchments.

As stated above, we calculate the F_{SCA} as a proxy of the snow regime. High F_{SCA} values (> 0.5) correspond to catchments with a seasonal snow cover (i.e., catchments where the snowmelt events are concentrated during late spring and summer snow-dominated) reveal a high F_{SCA} (> 0.40 , median $F_{SCA} = 0.51$). Gradually smaller F_{SCA} values refer to increasingly more ephemeral snowpacks, with intermittent snowmelt events during the winter season (Petersky and Harpold, 2018), as reflected by the spiky f_{SCA} timeseries of hybrid and rainfall-dominated catchments (Fig. 5).

Our results show a bell-shaped behavior of F_{yw}^* with varying F_{SCA} (Fig. 13a). Specifically, we observe a general increase of F_{yw}^* for F_{SCA} values roughly below 0.3. This result can be explained considering that especially in hybrid catchments (median $F_{SCA} = 0.28$), but partially also in rain-dominated catchments (median $F_{SCA} = 0.13$), streamflow receives relatively more young water from ephemeral snowpacks. These short-lived snowpacks melt during the winter season resulting in little delay between precipitation input and melt (i.e., no water aging in the snowpack), and corresponding meltwater potentially flows off quickly into the stream (reducing LFD, Fig. 14), e.g., in presence of a frozen surface soil layer. In fact, ephemeral and slightly thick snowpacks do not protect the underlying soil from freezing (Harrison et al., 2021; Rey et al., 2021). Even for low elevation locations ($< \approx 1500$ m a.s.l.), freezing conditions are regularly observed during winter (Keller et al., 2017).

For F_{SCA} values roughly higher than 0.3, we observe a decrease of F_{yw}^* with F_{SCA} ; here all the catchments of our data set are snow-dominated. The mechanisms at play here are: i) in catchments with seasonal snowpacks, streamflow receives

825 snowmelt in spring and summer that is at least partly older than 2-3 months (because part of the snow fell more than 3
months before the melt occurs). ii) The building up of a persistent, deep snowpack can promote deep vertical infiltration
830 during the main melt period, either by insulating the soil and thereby preventing/reducing freezing (Harrison et al., 2021;
Rey et al., 2021; Jasechko et al., 2016) or by gradual soil thawing during the melt period (Rey et al., 2021; Scherler et al.,
2010). The temporal dynamic of snow accumulation and melt supports the pivotal role of snowmelt in recharging
groundwater during summer in high-elevation environments (Cochand et al., 2019; Du et al., 2019; Flerchinger et al., 1992).
835 A similar result was also found for dolomitic catchments (such as BCC and OVA) by Lucianetti et al. (2020) , who revealed
different proportions of rain and snow contributions to the recharge of springs in the Dolomites, with a gradually higher
meltwater contribution in springs with increasing elevation. This role of snowmelt supports our analytical choice of
computing F_{yw}^* through the “direct input” approach, thus considering the snowpack as part of the catchment storage. In
addition, the potentially large shares of meltwater that recharge groundwater via deep vertical infiltration also result in old
water sustaining winter baseflow (Fig. S4): the persistent snowpack and the absence of a liquid water input favor a
groundwater storage emptying resulting in a longer winter low-flow period that increases LFD (Fig.14), thus reducing F_{yw}^* ,
as discussed in Section 4.3.

F_{SCt} is strongly correlated with the mean catchment elevation in our data set ($\rho_{\text{spearman}} = 0.97$, p-value < 0.01, Fig. 13b). A
posteriori, we could have considered mean elevation instead of F_{SCt} as a proxy for snowpack persistence. However, a priori,
840 it could be approximative to describe the snow cover persistence only with the increasing elevation: the persistence of snow
in a catchment also depends on catchment aspect, topography (Painter et al., 2023) snow-related and climatic characteristics.
In fact, catchments with very different characteristics (e.g., different elevation ranges, different areas etc.) can reveal a
similar mean elevation, but the snowpack persistence could considerably change. This is the reason why we decided to focus
on F_{SCt} that integrates these physical factors.

The above mechanisms are not able to explain the hydrological functioning of the glacier-dominated NBPV catchment,
845 which shows a very high F_{yw}^* and is categorized as an outlier among the snow-dominated catchments (Fig. 13a). The high
 F_{yw}^* of the high elevation glacier-covered (42%) catchment can be explained considering that the glacier-melt produces high
amounts of streamflow that transit the glacier-system very quickly during the summer, given generally fast englacial and
subglacial flow paths and the often limited water storage capacity in the glacier forefield (Müller et al., 2022; Saberi et al.,
850 2019; Jansson et al., 2003). Schmieder et al. (2019) also found a high young water fraction in an Austrian glacier-covered
(35%) catchment leading them to the conclusion that the basin behaves like a ‘Teflon basin’ with fast transmitted ice melt,
also if this behavior is differentiated in space.

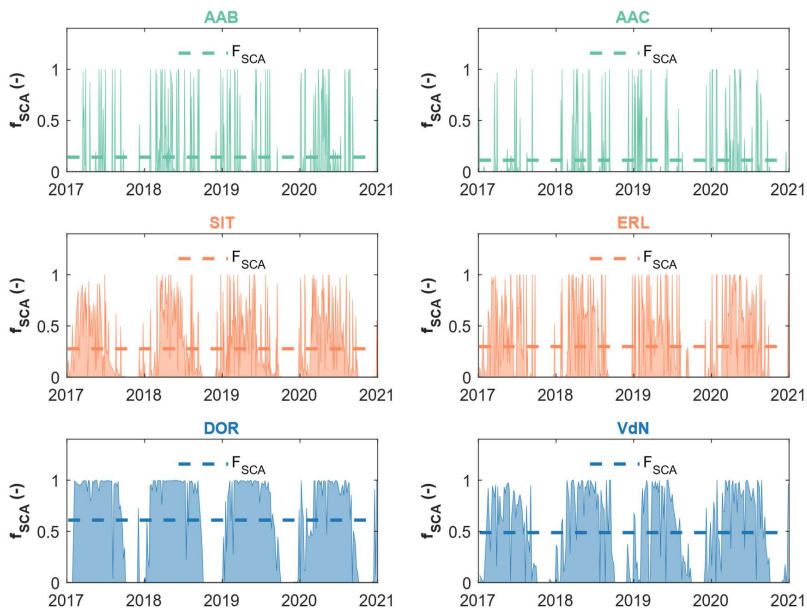


Figure 12 Timeseries of f_{SCA} for 6 representative study catchments (two for each hydro-climatic regime), illustrating the gradual increase of the F_{SCA} passing from rainfall-dominated to snow-dominated catchments.

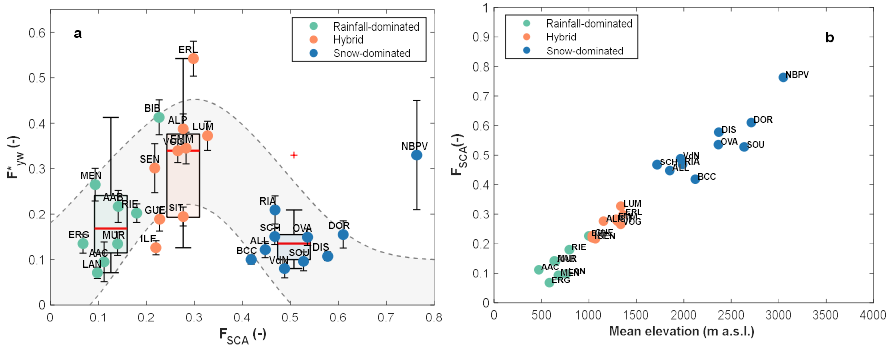
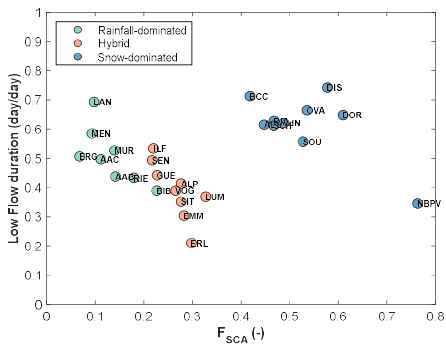


Figure 13 a) Young water fraction against F_{SCA} . The grey area represents the perceptual bell-shaped behaviour of F_{yw}^* with increasing F_{SCA} b) F_{SCA} against mean elevation.

855



860 **Figure 14** Low-flow duration (LFD) against F_{SCA}

865

Table 2 F_{yr}^* , F_{qd} , LFD, F_{bf} , F_{SCA} and WFI values for all the study catchments

ID (Regime)	F_{yr}^* (-)	F_{qd} (-)	LFD (d/d)	F_{bf} (-)	F_{SCA} (-)	WFI (-)
<u>AAB (R)</u>	<u>0.22</u>	<u>0.41</u>	<u>0.44</u>	<u>0.71</u>	<u>0.14</u>	<u>0.14</u>
<u>AAC (R)</u>	<u>0.10</u>	<u>0.99</u>	<u>0.50</u>	<u>0.73</u>	<u>0.11</u>	<u>0.15</u>
<u>ALL (S)</u>	<u>0.12</u>	<u>0.64</u>	<u>0.62</u>	<u>0.84</u>	<u>0.45</u>	<u>0.24</u>
<u>ALP (H)</u>	<u>0.39</u>	<u>0.61</u>	<u>0.41</u>	<u>0.69</u>	<u>0.28</u>	<u>0.06</u>
<u>BCC (S)</u>	<u>0.10</u>	<u>0</u>	<u>0.71</u>	<u>0.87</u>	<u>0.42</u>	<u>0.23</u>
<u>BIB (R)</u>	<u>0.41</u>	<u>0.61</u>	<u>0.39</u>	<u>0.65</u>	<u>0.23</u>	<u>0.06</u>
<u>DIS (S)</u>	<u>0.11</u>	<u>0.56</u>	<u>0.74</u>	<u>0.89</u>	<u>0.58</u>	<u>0.19</u>
<u>DOR (S)</u>	<u>0.16</u>	<u>0.24</u>	<u>0.65</u>	<u>0.85</u>	<u>0.61</u>	<u>0.06</u>
<u>EMM (H)</u>	<u>0.35</u>	<u>0.53</u>	<u>0.3</u>	<u>0.6</u>	<u>0.28</u>	<u>0.01</u>
<u>ERG (R)</u>	<u>0.14</u>	<u>0.50</u>	<u>0.51</u>	<u>0.75</u>	<u>0.07</u>	<u>0.05</u>
<u>ERL (H)</u>	<u>0.54</u>	<u>0.74</u>	<u>0.21</u>	<u>0.50</u>	<u>0.30</u>	<u>0.01</u>

<u>GUE (H)</u>	<u>0.19</u>	<u>0.8</u>	<u>0.44</u>	<u>0.71</u>	<u>0.23</u>	<u>0.07</u>
<u>ILF (H)</u>	<u>0.13</u>	<u>0.69</u>	<u>0.53</u>	<u>0.77</u>	<u>0.22</u>	<u>0.12</u>
<u>LAN (R)</u>	<u>0.07</u>	<u>0.98</u>	<u>0.69</u>	<u>0.87</u>	<u>0.10</u>	<u>0.40</u>
<u>LUM (H)</u>	<u>0.37</u>	<u>0.90</u>	<u>0.37</u>	<u>0.66</u>	<u>0.33</u>	<u>0.08</u>
<u>MEN (R)</u>	<u>0.27</u>	<u>0.93</u>	<u>0.59</u>	<u>0.79</u>	<u>0.09</u>	<u>0.18</u>
<u>MUR (R)</u>	<u>0.13</u>	<u>0.62</u>	<u>0.53</u>	<u>0.77</u>	<u>0.14</u>	<u>0.19</u>
<u>NBPV (S)</u>	<u>0.33</u>	<u>0.24</u>	<u>0.35</u>	<u>0.7</u>	<u>0.76</u>	<u>0.00</u>
<u>OVA (S)</u>	<u>0.15</u>	<u>0.41</u>	<u>0.66</u>	<u>0.85</u>	<u>0.54</u>	<u>0.21</u>
<u>RIA (S)</u>	<u>0.21</u>	<u>0.43</u>	<u>0.63</u>	<u>0.84</u>	<u>0.47</u>	<u>0.11</u>
<u>RIE (R)</u>	<u>0.2</u>	<u>0.21</u>	<u>0.43</u>	<u>0.68</u>	<u>0.18</u>	<u>0.07</u>
<u>SCH (S)</u>	<u>0.15</u>	<u>0.62</u>	<u>0.61</u>	<u>0.85</u>	<u>0.47</u>	<u>0.20</u>
<u>SEN (H)</u>	<u>0.30</u>	<u>0.5</u>	<u>0.49</u>	<u>0.75</u>	<u>0.22</u>	<u>0.24</u>
<u>SIT (H)</u>	<u>0.19</u>	<u>0.54</u>	<u>0.35</u>	<u>0.68</u>	<u>0.28</u>	<u>0.07</u>
<u>SOU (S)</u>	<u>0.10</u>	<u>0</u>	<u>0.56</u>	<u>0.82</u>	<u>0.53</u>	<u>0.01</u>
<u>VdN (S)</u>	<u>0.08</u>	<u>0.49</u>	<u>0.62</u>	<u>0.84</u>	<u>0.49</u>	<u>0.04</u>
<u>VOG (H)</u>	<u>0.34</u>	<u>0.48</u>	<u>0.39</u>	<u>0.66</u>	<u>0.27</u>	<u>0.07</u>

4.5 Process interplay along elevation: perceptual model

870

The identified key drivers of young water fractions for rainfall-dominated, hybrid and snow-dominated catchments can conveniently be summarized into a perceptual model of the involved hydrological processes and their seasonal interplay (Fig. 15).

875

High-elevation catchments are characterised by long winter low-flow periods, resulting from the build-up of a seasonal snowpack, and sustained by the emptying of groundwater (or old water) storage. Accordingly, such storage releases stored water, mainly old meltwater, for prolonged periods where the snowpack can last for several months (typically from December to early April) before releasing water during the melting season. Such seasonal snowpack can protect the underlying soils from freezing, favouring meltwater infiltration and groundwater recharge. From this viewpoint, snowpack is considered as part of the catchment storage and there is a thin line between groundwater and meltwater in snow-dominated catchments. Snowmelt or rain events push out old meltwater to the stream during summer, as suggested by the relatively high amount of daily baseflow during the melting season. During this period, the high catchment wetness might even lead to saturation and thereby favour fast flow paths of meltwater or rainwater, which in turn can temporarily increase the young

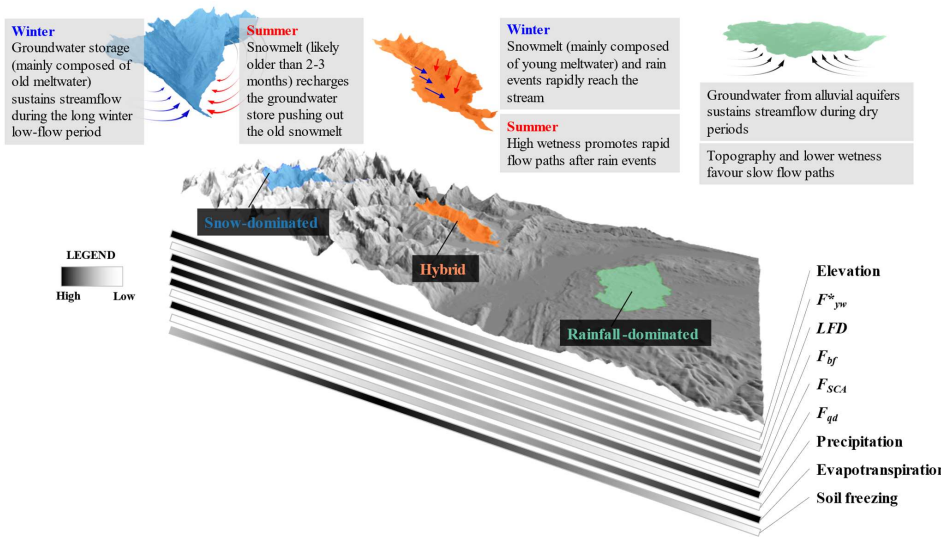
880

water fraction. Despite this increase during high-flow periods, the prevailing winter low-flow periods in such systems lead to a reduction of the average annual young water fraction.

885 In catchments with an ephemeral snowpack, at lower elevations, snowmelt events occur regularly during winter such that water released from the corresponding short-lived snowpack is likely younger than 3 months. Moreover, ephemeral snowpacks do not protect the underlying soils from freezing and rapid flow paths can emerge during episodic or long-term soil surface freezing, increasing the young water fraction. The high F_{yw}^* of such systems is also explained by the simultaneity of snowmelt and rain events during extended parts of the year (leading to large volume of annual precipitation)
890 and the relatively low (compared to rainfall-dominated catchments) evapotranspiration. Both processes increase the catchments wetness and reduce the low-flow periods length.

Finally, at the lowest elevations, lower amounts of precipitation and higher evapotranspiration favour longer low-flow periods, mainly sustained by old groundwater from alluvial aquifers, which lead to both a F_{yw}^* and catchment wetness reduction. Further, the relatively flat topographies at the lowest elevations favour slow flow paths increasing the transit times
895 of water.

How well current hydrological models can represent the interplay of these processes along elevation gradients is left for future research, but our perceptual model builds a solid basis for an improvement of theory-driven models (Clark et al., 2016).



900 **Figure 15** Perceptual model of the hydrological processes that drive the young water fraction variations with elevation. This model emerges from our analysis and harmonizes these results with those of previous studies. For snow-dominated and hybrid catchments, we indicate the dominant processes, occurring during summer and during winter, that lead to low and high F_{yw}^* , respectively.

905 **5 Conclusion**

This study proposes a conceptualization of the processes behind changes in young water fraction (F_{yw}^*) with elevation, defined here following Kirchner (2016a) as water that is younger than 2-3 months. The analysis is based on young water fractions for a set of 27 study catchments located in Switzerland and Italy which span a wide range of geological and hydro-climatic conditions. Our analysis focuses on mountainous catchments to fill the knowledge gap referring to the surprisingly low young water fractions at high elevations (> 1500 m a.s.l.), but we have also considered catchments at lower elevations to obtain a complete picture of the dominant hydrological processes at different elevations.

910 We have focused on variables and processes that were not previously considered for explaining elevation gradients of young water fraction. We have investigated the role of i) the groundwater storage potential ii) the catchment storage contribution to the stream iii) the low-flow duration iv) the snowpack persistence. Our results suggest that ii) iii) and iv) are connected to each other: low-flow periods are generally sustained by old water deriving from the catchment storage and the length of such periods is driven by the snowpack persistence at high elevations. The proportion of low-flow periods during the period of isotope sampling strongly influences the amount of old water contributing to the stream, thus reducing the estimated F_{yw}^* .

920 Consequently, the low-flow duration, which varies with elevation, can be retained as driver of the F_{yw}^* changes with elevation. Given the importance of low-flow periods, we have also investigated the role of groundwater storage potential, represented here by the portion of catchment area covered by Quaternary deposits. Our results suggest that this analysis should be completed with more detailed geological information e.g., the geology and topography of bedrock, the fraction of fractured bedrock and the deposits' thickness, which is challenging to retrieve from geological data set. We have finally harmonized the results of this analysis in a perceptual model that describes a framework for how hydrological processes control the F_{yw}^* according to elevation, laying the foundations for an improvement of theory-driven models.

925 The strong complementarity between F_{yw}^* and the average fraction of baseflow obtained for our data set suggests that F_{yw}^* could be estimated starting from automated baseflow separation techniques for catchments in which stable water isotopes measurements are not available. This complementarity should however be validated in future work, considering e.g., alternative baseflow separation techniques and different hydro-climatic conditions.

930 Finally, the conceptualization of the hydrological processes described in this paper do not fit the high young water fraction of the single glacier-dominated catchment of our data set. In conclusion, we encourage future studies to compare and to collect isotopic data from glacier-dominated catchments to better understand the processes in such systems that, under glacier retreat due to climate change, will see a gradual transition to purely snow-dominated systems.

935 *Data availability.* Time series of both $\delta^2\text{H}$ and $\delta^{18}\text{O}$ in streamflow and precipitation for the 22 Swiss catchments investigated by von Freyberg et al. (2018) are available in the data repository Zenodo at <https://zenodo.org/record/4057967#.Y00oMHZBxPY> (Staudinger et al., 2020). Meteorological, hydrological and isotope data of VdN, BCC and NBPV catchments are available at: <https://onlinelibrary.wiley.com/action/downloadSupplement?doi=10.1002%2Fhyp.13937&file=hyp13937-sup-0009-Supinfo2.zip>. For the existing data set, we used the values of F_{yw}^* (direct-input) reported in Fig. 4c of von Freyberg et al.

940 (2018), kindly provided by the corresponding author, and in Table 6 of Ceperley et al. (2020) with associated errors. Daily discharge data for the ERL, LÜM and VOG catchments are provided by the *Swiss Federal Institute for Forest, Snow and Landscape research (WSL)*, Birmensdorf, Switzerland. Streamflow data for the AAB and GUE catchments are provided by the *Office for Waste, Water, Energy and Air (WWEA)* of the Canton of Zurich and by the *Office for Water and Waste* of the Canton of Bern, respectively. Daily discharge data of the remaining 17 Swiss catchments studied by von Freyberg et al.

945 (2018) are provided by the *Swiss Federal Office for the Environment (FOEN)*.

950 The .shp of the AAB, GUE, ERL, LÜM and VOG catchments boundaries are available from the data repository Zenodo at <https://zenodo.org/record/4057967#.Y00oMHZBxPY> (Staudinger et al., 2020). The .shp of NBPV, BCC and VdN catchments, are provided by Dr. Giulia Zuecco and Dr. Anthony Michelon (University of Lausanne, Switzerland) as personal communication. The DOR and SOU catchments boundaries are delineated in a GIS environment using the 10-m resolution Digital Elevation Model (DEM) available from the *Aosta Valley Regional Geoportail*. Finally, the catchment boundaries of

the remaining 17 Swiss catchments investigated by von Freyberg et al. (2018) are directly obtained from the *Swiss Federal Office for the Environment (FOEN)*.

Quaternary cover for all Swiss catchments has been calculated using the Geological Atlas of Switzerland (GeoCover data set, 1:25000 scale) available from the *Federal Office of Topography swisstopo*. For the DOR and SOU catchments the vectorized Valsavaranche geological map (1:100000 scale) is provided by the *Cartography Office of SCT Geoportal*. For the NBPV and BCC catchments the .shp of unconsolidated sediments is provided by Dr. Giulia Zuecco.

Our results highlight a different median F_{yw} for each hydro-climatic regime (Fig. 6), with similar low values for rainfall-dominated catchments (median F_{yw} of 0.16) and snow-dominated catchments (median F_{yw} of 0.14) but much higher values for hybrid catchments (median F_{yw} of 0.32), which in addition shows higher dispersion (Fig. 6). We observe a general increase of F_{yw} as long as the F_{SCA} remains below roughly one-third or more exactly 0.38 (median f_{SCA} for hybrid catchments) and a subsequent lowering of F_{yw} when F_{SCA} is higher than this threshold. In fact, considering only catchments with a $F_{SCA} < \sim 0.38$, we obtain a statistically significant positive correlation between F_{yw} and F_{SCA} ($\rho_{\text{spearman}} = 0.72$, p-value < 0.01). In contrast, catchments with a $F_{SCA} > \sim 0.38$, aside from NBPV, show a negative statistically significant correlation ($\rho_{\text{spearman}} = -0.5$, p-value < 0.1). We exclude the NBPV glacier-dominated catchment since its F_{SCA} - and F_{yw} -relationship is an outlier compared to the other snow-dominated catchments. Note that ERL and ALP catchments are included in both correlations since their F_{SCA} is very close to 0.38. Thus, it is difficult to reliably allocate these catchments to either the “rising” or “falling” limbs of the F_{yw} - F_{SCA} relationship as observable in Fig. 6.

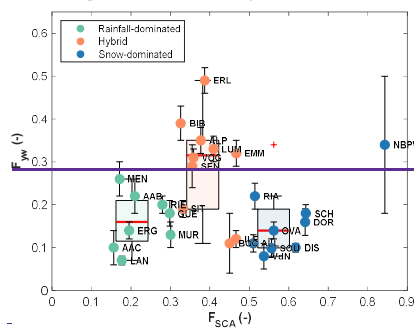


Figure 6. F_{yw} against F_{SCA} . The vertical bars are as in Fig. 4b. The boxplots show the median, quartiles, and whiskers (extending to the most extreme data points not considered outliers, the latter indicated with the '+' red symbol) of the F_{yw} values per regime type, centered on the corresponding median f_{SCA} value per regime type (0.20, 0.38 and 0.56).

4.3.2 — The role of quaternary deposits

To advance our understanding of the process that drives F_{yw} according to elevation gradient, we analyze the correlation between the fraction of unconsolidated deposits (F_{qu}) and the young water fraction (Fig. 7), assuming that groundwater is

975 stored in unconsolidated sediments. We exclude the SOU and BCC catchments from our analysis, which show $F_{qd} = 0$.
 Considering only the 9 snow-dominated catchments, i.e., the group having the features as close as possible to those used by
 Arnoux et al. (2021), we find a Spearman rank correlation coefficient of -0.5 with a p-value of 0.22, meaning a negative, but
 not statistically significant correlation between F_{yw} and F_{qd} . F_{yw} values of the 10 hybrid catchments reveal a positive, but non-
 significant correlation with unconsolidated sediments ($\rho_{\text{Spearman}} = 0.4$, p-value = 0.29). Finally, rainfall-dominated catchments
 980 show a negative, non-significant correlation ($\rho_{\text{Spearman}} = -0.52$, p-value = 0.2).

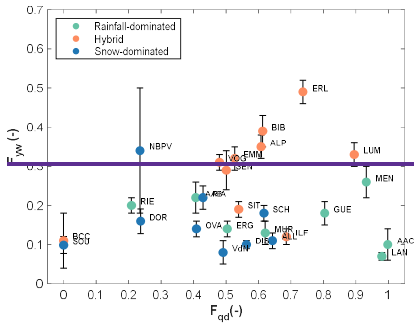


Figure 7. Plot of F_{yw} against the fraction of quaternary deposits (F_{qd})

4.3.3 — Groundwater contribution to streamflow: WFI and F_{bf} related with F_{yw}

985 Analysis by Arnoux et al. (2021) revealed that the fraction of quaternary deposits is positively correlated with the low flow
 indicators (e.g., WFI) in high elevation catchments. This evidence indicates that catchments with high WFI receive an
 important contribution from groundwater (Arnoux et al., 2021). This is also confirmed by our dataset (Fig. 8a). Indeed, if we
 look at snow-dominated catchments, always removing the SOU catchment since it shows a $F_{qd} = 0$, we find a positive and
 statistically significant correlation ($\rho_{\text{Spearman}} = 0.67$ p-value < 0.1) of F_{qd} with the WFI . Conversely, we do not find statistically
 significant correlations for hybrid (negative correlation) and rainfall-dominated (positive correlation) catchments. In
 990 exchange, WFI is negatively and significantly correlated with the young water fractions of the entire dataset ($\rho_{\text{Spearman}} = -0.40$
 p-value < 0.1) as shown in Fig. 8b.

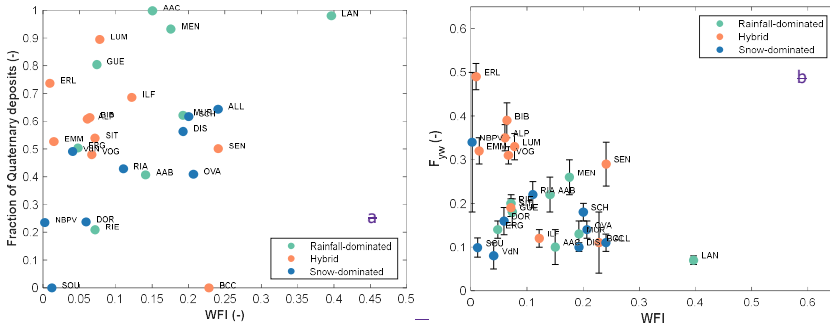


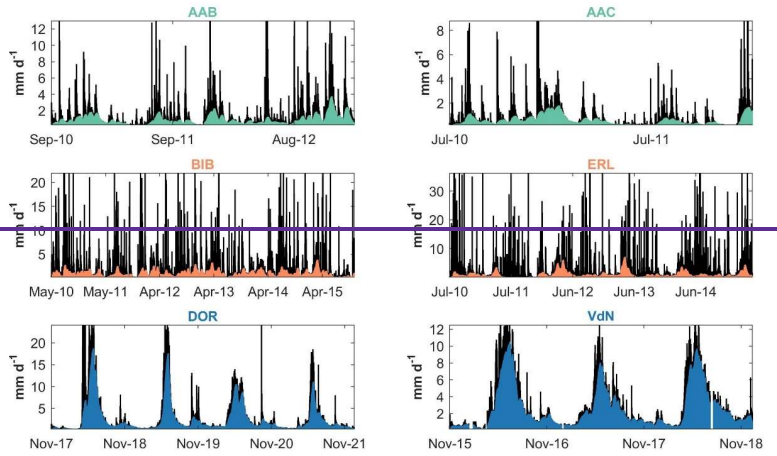
Figure 8. a) Fraction of quaternary deposits plotted against WFI; b) Young water fraction plotted against WFI.

As described in Section 3.5, we apply the baseflow filter of Duncan et al. (2019) to the daily discharge data of the 27 study catchments for having a more physical evaluation of the groundwater contribution to streamflow. The resulting baseflow time series are reported in Fig. 9 for the selected six representative study catchments (time series for all the study sites are available in the Supplementary Material, Fig. S3).

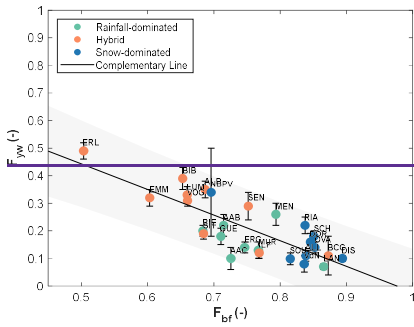
To directly compare the F_{yw} with the amount of baseflow, considered here as a proxy for groundwater, we calculate the average fraction of baseflow (F_{bf}) as reported in Section 3.5. We obtain a strongly negative and significant correlation of F_{yw} with F_{bf} ($\rho_{\text{Spearman}} = -0.75$, $p\text{-value} < 0.01$) as shown in Fig. 10. The F_{bf} is generally lower for hybrid catchments (median F_{bf} of 0.67) than for rainfall-dominated catchments (median F_{bf} of 0.74) and snow-dominated catchments (median F_{bf} of 0.84). Moreover, the fit of a line of F_{yw} as a function of F_{bf} points (e f tool, Matlab R2019b) demonstrates a complementary relationship ($R^2 = 0.65$):

$$F_{yw} = -(0.93 \pm 0.19)F_{bf} + (0.91 \pm 0.22), \quad (9)$$

Interestingly, we find that the NBPV catchment has a lower F_{bf} (≈ 0.7) if compared to the median F_{bf} of catchments belonging to the same regime. All the results in terms of median values per regime are summarized in Table 3. The full results table (Table S1) for all catchments is available in the Supplementary Material.



1010 **Figure 9.** Baseflow separation for six representative study catchments using the Duncan (2019) filter. The black area represents the daily discharge, while the coloured area represents the estimated daily baseflow.



1015 **Figure 10.** Young water fraction plotted against fraction of baseflow. Grey area represents the 95% prediction bounds of a linear regression of F_{yw} on F_{br} .

Table 3. Summary table with all the results in terms of median values with associated Inter-Quartile Range (IQR) for each hydro-climatic regime.

	rainfall-dominated		hybrid		snow-dominated	
	median	IQR	median	IQR	median	IQR
$F_{yw}(-)$	0.16	0.10	0.32	0.16	0.14	0.09
$F_{hy}(-)$	0.74	0.07	0.67	0.10	0.84	0.02
$WFI(-)$	0.15	0.11	0.07	0.06	0.11	0.17
$F_{qd}(-)$	0.71	0.50	0.57	0.19	0.43	0.34
$F_{SCA}(-)$	0.20	0.11	0.38	0.09	0.56	0.11
$Q_{June}/Q_{DJF}(-)$	0.26	0.10	0.47	0.41	3.74	2.95

5—Discussion

5.1—The new hydro-climatic regime classification

For each of the three hydro-climatic regimes, it is possible to define an average characteristic shape of the monthly hydrograph (Fig. 11). A shift of the monthly hydrograph peak of about 1.5 months is observed passing from rainfall-dominated (peak in March) to hybrid catchments (peak in mid-April) and then, passing from a hybrid to a snow-dominated (peak in June) regime (Fig. 11). This “flow peak shifting” is a clear sign of the increasing predominance of snowmelt in the streamflow generation processes and is at the basis of Pardé Coefficient-based regime classifications. Accordingly, the value of the classification proposed here is not to shed new light on streamflow dynamics but to objectively connect the streamflow regime shape to summer-to-winter streamflow ratios and to the mean snow cover extent. The new classification scheme can be applied outside Switzerland and the objective and explicative classifiers, on which it is based, allow the study of regime changes (e.g., from snow-dominated to hybrid) that will become increasingly more apparent under climate change (Lucianetti et al., 2020; Harrison et al., 2021).

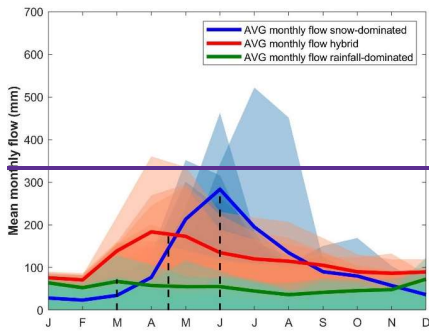


Figure 11. Coloured areas represent the monthly flow of each study catchment. The solid lines indicate the average monthly flow for each hydro-climatic regime, thus defining a characteristic shape of the monthly hydrograph for each of such regimes. Dashed black lines show the month in which, on average, the peak-flow is observed for each hydro-climatic regime.

5.2 — A perceptual model: snowpack persistency favours increasing water age.

A perceptual model that describes the theoretical behavior of young water fraction with varying F_{SC4} emerges from our analysis and harmonizes the results of this work with that of previous studies.

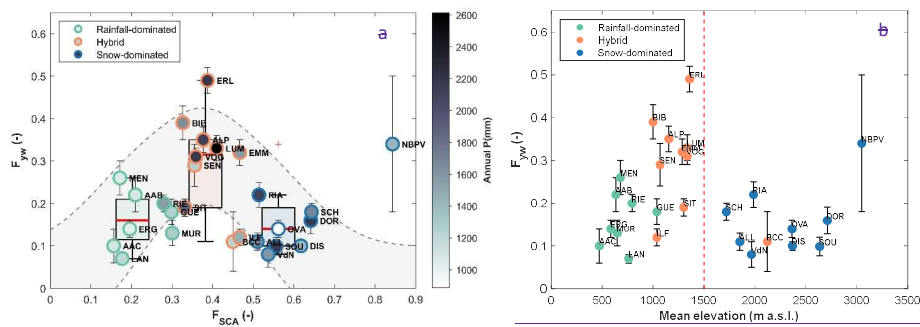
A plot of F_{SC4} against F_{yw} (Fig. 12a) shows a bell-shaped behavior (which we visualize with the grey shade in Fig. 12a) that suggests the interplay of two different trends: a positive trend as long as $F_{SC4} < \approx 0.38$ and a negative trend for $F_{SC4} > \approx 0.38$. This threshold (that is the median f_{SC4} of hybrid catchments) splits the hybrid regime in two sub-classes.

The first sub-class (elevation $< \approx 1500$ m a.s.l.) is mainly influenced by the rain-dominated regime. Accordingly, the rising limb of the bell-shaped curve can be primarily explained by the increase of precipitation and slope with elevation (Fig. 12a, Fig. 4a) and the reduction of evaporation with elevation due to reduced temperatures (Goulden et al., 2012). As elevation increases, these factors favor an ever-growing lateral and longitudinal connectivity (Tromp van Meerveld and McDonnell, 2006; McDonnell, 2013; McDonnell et al., 2021) producing wetness conditions that promote rapid flow paths: the young water fraction increases but also groundwater recharge; this promotion of groundwater recharge is visible in a plot of winter baseflow against elevation (Fig. S4). In addition, higher order channels, higher up, are more rarely activated than lower order channels that are more often active (Botter et al., 2021; Durighetto et al., 2022). Therefore, it is more likely that lower order channels are draining more old water than the temporary activated higher order channels: water age decreases with elevation when catchments reveal a negligible or a shallow, possibly ephemeral, snowpack. In fact, the limited number of snowfall days and mid-winter melt reduce the snow accumulation in the lower elevation sub-class of hybrid regimes. Such a snowpack does not protect the underlying soils from freezing (Harrison et al., 2021). Even for low elevation locations ($< \approx 1500$ m a.s.l.), freezing conditions are regularly observed during winter (Keller et al., 2017): such conditions can lead to soil

freezing thereby inhibiting infiltration and favoring rapid flow paths during mid-winter melt events, with subsequent increase of F_{ym} .

In contrast, the second sub-class (elevation $> \approx 1500$ m a.s.l.) of hybrid catchments is increasingly influenced by the snow-regime. Here, the building up of a persistent, deep snowpack can promote deep vertical infiltration by insulating the soil and thereby preventing freezing (Jasechko et al., 2016; Harrison et al., 2021). The resulting effect on water partitioning between the surface and the subsurface has however to be analyzed in light of the temporal concentration of water input on the snowmelt period and remains largely unexplored to date (Rey et al., 2021). Despite of this, the temporal dynamic of snow accumulation and melt and its effect on deep infiltration supports the pivotal role of snowmelt in recharging groundwater during summer in high elevation environments (Flerchinger et al., 1992; Cochand et al., 2019; Du et al., 2019). Moreover, the analysis of Lucianetti et al. (2020) revealed different varying proportions of rain and snow contributions to the recharge of springs in the Dolomites according to elevations. Specifically, they observed a gradually higher snowmelt contribution in springs passing from roughly 46% below 2000 m a.s.l to nearly 72% above 2500 m a.s.l. To advance our understanding of F_{ym} along elevation gradients, we also need to ask how and when groundwater storage contributes to streamflow. Here, another crucial function of the seasonal snowpack comes into play: it favors the emptying of the groundwater storage over long winter recession periods. In some snow-dominated environments, the seasonal snow cover can persist for more than six months, and the streams correspondingly show a low flow regime resulting from absence of rain and melt input, with minimum flow during winter decreasing below 0.5 to 1 mm/d for the highest locations (Fig. S5). It is assumed that these low-flow periods, generally consistent from year to year because of the annual temperature cycle, are sustained by the groundwater storage that provides resilience to Alpine rivers (Hayashi, 2020). This groundwater (or old water) contribution to streamflow during the winter period increases the age of streamwater. In addition, high elevation catchments can reveal winter low flow periods that are significantly longer than their high flow periods (Hayashi, 2020). In conclusion, this low-flow period could strongly influence the water age, thereby decreasing the F_{ym} .

The above mechanisms are summarized in the perceptual model reported in Fig. 13 also indicating which are the dominant processes over the winter and summer seasons. This model is, however, not able to explain the NBPV catchment hydrological functioning, which is classified as snow-dominated according to our classification criterion, but our criterion does not consider the influence of glaciers. The NBPV catchment area is 42% glacier covered, so it is probable that this catchment should belong to a fourth class of "glacier-dominated" catchments (in fact, it is detected as an outlier: see blue boxplot in Fig. 12a). Such catchments could show fast flow paths and small storages as e.g. discussed in the work of Jansson et al. (2003), reviewing glacier-dominated environments. Moreover, reduced baseflow during winter can be related to increasingly high temperatures causing the glaciers retreat, thus reducing and anticipating the glacier melt fluxes that possibly recharge groundwater (Hayashi, 2020).



1090 **Figure 12.** a) Theoretical behavior of young water fraction with varying F_{SCA} indicated by the grey area b) F_{yw} as function of mean catchment elevation. The dashed red line indicates the threshold elevation above which the F_{yw} -reset is observed.

5.3 — The role of unconsolidated sediments in increasing or decreasing water age

1095 We have achieved correlation that is not statistically significant between F_{qt} and F_{yw} that can be explained considering that unconsolidated sediments are not the only groundwater storage contribution to the stream during low-flow periods in such environments. In steeper catchments, additional storage is provided by the bedrock fractures (Gleeson et al., 2014; Jasechko et al., 2016; Martin et al., 2021) and by the bedrock geology which has influence on groundwater retention capacity (Hayashi, 2020). However, necessary data is elusive.

1100 The positive correlation between F_{yw} and F_{qt} in hybrid catchments can be explained by two mechanisms: i) high baseflow points towards system saturation being high, which favors connectivity and ii) ephemeral snowpacks can favor freezing phenomena inhibiting winter snowmelt infiltration and thereby favoring fast flow processes (Harrison et al., 2021). Concluding, we stress that more catchments and more geological information would be required to statistically validate these observations.

1105

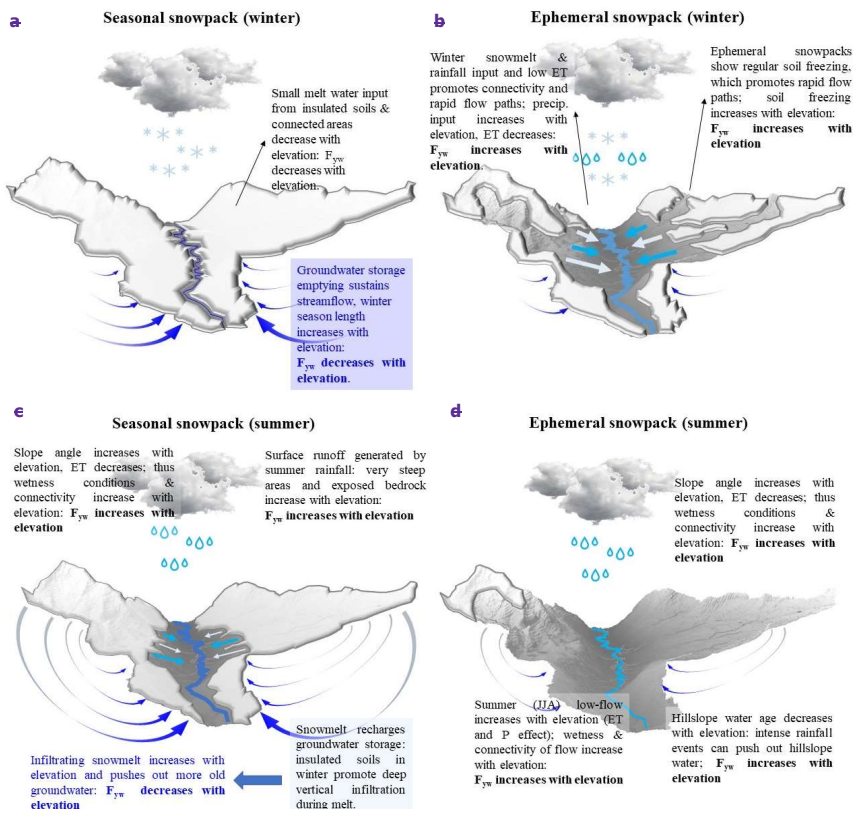


Figure 13. Perceptual model of different hydrological functioning of catchments characterized by ephemeral snowpacks, in panels b (winter) and d (summer), and by seasonal snowpacks, panels a (winter) and c (summer).

5.4 — Groundwater contribution to streamflow is the key to understand F_{yw} gradients

We have tested here if the counterintuitive low F_{yw} obtained for high elevation catchments depends on the groundwater contribution to streamflow and if the results are consistent with our perceptual model. We obtain a statistically significant negative correlation between F_{yw} and F_{bf} (Fig. 10) and the linear fit of the points suggests that F_{bf} is roughly the one's

complement of F_{yw} . This result clearly indicates that the observed patterns of F_{yw} are related to water partitioning between the surface and the subsurface. Moreover, this complementarity gives a further physical meaning for the estimated baseflow in our data set: the estimated baseflow should correspond to water with transit times higher than roughly 0.2 years.

We find the highest F_{bf} for snow-dominated catchments confirming the presence of high subsurface storage, contributing to streams, in high-elevation catchments (Staudinger et al., 2017). Moreover, the annual baseflow is strongly positively correlated with the F_{SCA} ($\rho_{\text{snowmelt}} = 0.81$, p-value < 0.01) suggesting a major groundwater contribution with increasing snow cover persistency (Fig. S6).

The major dispersion of F_{bf} we find in hybrid catchments supports the idea that such catchments can reveal a different hydrological functioning depending on whether they are mainly influenced by the rain or snow regime. The hydro-climatic regime is generally a good indicator of the proportion of young water that contributes to streamflow, with a few exceptions though. Interestingly, the F_{bf} offers an explanation for these exceptions. For example, the BCC catchment is classified as hybrid, but it reveals a low F_{yw} (0.11) that is comparable with those obtained for snow-dominated catchments (median $F_{yw} = 0.14$). In fact, BCC reveals a F_{SCA} of 0.45, very close to the threshold of 0.5 for being classified as snow-dominated (Table 2) and a high F_{bf} (0.87) underlining the dominant role of groundwater in the streamflow generation. This result is consistent with previous findings of Penna et al. (2016) for this catchment: they have shown that, on average, from 80% to 98% of BCC discharge is constituted by pre-event water (assumed to represent groundwater).

Another special case is the NBPV catchment: it is an outlier in the F_{yw} - F_{SCA} space (Fig. 12a, i.e., the perceptual model is not able to explain its high F_{yw}) but it results to be in line with the other catchments in the F_{yw} - F_{bf} space (Fig. 10) and its relatively high F_{yw} (0.34) can reasonably be explained with a relatively low F_{bf} (0.70, i.e. a relatively low groundwater contribution to streamflow).

Therefore, we can conclude that the contribution of groundwater storage to streamflow, which is driven by snowpack duration, can be considered as the best explanatory variable of the F_{yw} elevation gradients.

61 Conclusion

This paper demonstrates, based on a new collection of observations of high-elevation catchments from both published datasets and new field observations, that Alpine young water fractions, F_{yw} , show a topographic pattern that is characterized with an increase to about 1500 m a.s.l., and a decrease thereafter. We provide here an explanation for this pattern, thereby clarifying why F_{yw} is low in high-elevation catchments, filling a knowledge gap expressed in previous studies. All the study catchments have been classified in three categories: rainfall-dominated, hybrid or snow-dominated. We do this through a new classification scheme that can be applied using objective and parsimonious classifiers: the summer/winter discharge ratio ($Q_{\text{June}}/Q_{\text{DJF}}$) and the fractional snow cover area (F_{SCA}). These classifiers strongly correlate; therefore, it is possible to use the easy-to-calculate $Q_{\text{June}}/Q_{\text{DJF}}$ for obtaining a first-order estimate of F_{SCA} through the exponential relationship proposed in this paper.

We focus on the correlations between F_{yw} and three selected variables: the fraction of quaternary deposits, F_{qd} , F_{SCA} , and the fraction of baseflow, F_{bf} . Additionally, we consider the Winter Flow Index (*WFI*) for comparing our results about the groundwater contribution to streamflow with those of previous works.

The fraction of quaternary deposits (F_{qd}), assumed to store groundwater, does not produce a statistically significant correlation with F_{yw} ; however, this analysis should be completed with more detailed geological information, e.g., the bedrock geology or the fraction of fractured bedrock, which is hard to retrieve in geological data set.

The relationship between F_{yw} and F_{SCA} shows a bell-shaped curve that suggests the activation of different hydrological processes depending on the snowpack duration (ranging from ephemeral to seasonal). Building from this observation, we develop a perceptual model of how snow persistency explains F_{yw} during winter and summer along topographic gradients: during winter, at elevations with an ephemeral snowpack ($< \approx 1500$ m a.s.l.), high system wetness and soil freezing favor rapid flow paths leading to high F_{yw} ; at elevations with a seasonal snowpack ($> \approx 1500$ m a.s.l.), there is almost no water input during winter and streamflow is fed by progressively emptying groundwater storage, leading to low F_{yw} . These seasonal snowpacks insulate soils, thereby promoting deep vertical infiltration on the snowmelt onset and supporting the pivotal role of snowmelt in recharging groundwater storage in high mountain environments during summer. This recharge leads to high baseflow throughout the year, especially during winter, and only few streamflow events characterized by fast flow paths. Since winter low flow periods can be longer than high flow periods in snow-dominated catchments, such periods influence the water age at annual scale and thereby lead to decreasing F_{yw} with winter duration (i.e., with elevation).

This perceptual model is corroborated by the high negative correlation between F_{bf} and F_{yw} , which indicates a key role of groundwater in streamflow generation processes and further confirmed by the negative and significant correlation between *WFI* and F_{yw} . Nevertheless, our model is not able to explain the hydrological functioning of the single glacier-dominated catchment in our dataset, even if we can explain its high F_{yw} by the relatively low groundwater contribution (i.e., low F_{bf}). Thus, further research is necessary to conceptualize the processes of such systems that under glacier retreat will see a gradual transition to purely snow-dominated systems.

Data availability.

DOR and SOU data are available from Alessio Gentile upon reasonable request. Data of the remaining 25 catchments are freely available online and all the data sources are cited in the manuscript

Code availability. A GEE script for calculating Snow Cover Area and Cloud Cover Area time series over a region of interest has been made available at: <https://code.earthengine.google.com/8239cfe7aab498180e5c42475023cb80?noload=true>. A Matlab © code with the implementation of the Duncan (2019) baseflow filter is available with the Supplementary Material of this article.

Supplement. The supplement related to this article is available online at

Author contributions. AG, NC, BS and SF identified the research gap, defined the methodology, developed the perceptual model; and prepared the paper. AG analyzed the data set. DG, DC, MP and SF collected the water samples for the DOR and SOU catchments. GZ analyzed spatial data related to NBPV and BCC catchments. All authors revised the manuscript and gave final approval to the submitted version.

Competing interests. The authors declare that they have no conflict of interest.

Acknowledgements. This work was supported by the “PRIN MIUR 2017SL7ABC_005 WATZON Project” and the “MIUR - Excellence Department: National funds allocated to the DIST department”. We warmly thank the “COST Action CA19120 - WATSON (WATER isotopeS in the critical zONe)” for the acceptance of the application procedure for one Virtual Mobility (VM) and one Short Term Scientific Mission (STSM). Both activities allowed to speed up the planning and conceptualization of this work as well as to stimulate the collaboration, the sharing of data and ideas. Last but not least, we acknowledge the support of the Valsavarenche Municipality and the Gran Paradiso National Park. The authors thank Dr. Chiara Marchina (University of Padova, Italy) for the isotopic analyses of DOR and SOU samples. Finally, we thank Jana von Freyberg and one anonymous referee for their comments that helped to improve the paper significantly.

76 References

Aalstad, K., Westermann, S., and Bertino, L.: Evaluating satellite retrieved fractional snow-covered area at a high-Arctic site using terrestrial photography, *Remote Sens.: Environ., Sensing of Environment*, 239, 111618, <https://doi.org/10.1016/j.rse.2019.111618>, 2020.

Addor, N., Rössler, O., Köplin, N., Huss, M., Weingartner, R., and Seibert, J.: Robust changes and sources of uncertainty in the projected hydrological regimes of Swiss catchments, *Water Resour. Res.*, 50, 7541–7562, <https://doi.org/10.1002/2014WR015549>, 2014.

Andermann, C., Longuevergne, L., Bonnet, S., Crave, A., Davy, P., and Gloaguen, R.: Impact of transient groundwater storage on the discharge of Himalayan rivers, *Nat. Nature Geosci.*, 5, 127–132, <https://doi.org/10.1038/ngeo1356>, 2012.

Antoniazza, G., Nicollier, T., Boss, S., Mettra, F., Badoux, A., Schaefli, B., Rickenmann, D., and Lane, S. N.: Hydrological Drivers of Bedload Transport in an Alpine Watershed, *Water Resour. Res.*, 58, e2021WR030663, <https://doi.org/10.1029/2021WR030663>, 2022.

Arnoux, M., Brunner, P., Schaefli, B., Mott, R., Cochand, F., and Hunkeler, D.: Low-flow behavior of alpine catchments with varying quaternary cover under current and future climatic conditions, *J. Hydrol., Journal of Hydrology*, 592, 125591, <https://doi.org/10.1016/j.jhydrol.2020.125591>, 2021.

- 1215 Baraer, M., McKenzie, J. M., Mark, B. G., Bury, J., and Knox, S.: Characterizing contributions of glacier melt and groundwater during the dry season in a poorly gauged catchment of the Cordillera Blanca (Peru), in: *Advances in Geosciences, 4th EGU Alexander von Humboldt Conference "The Andes: Challenge for Geosciences" - 4th Alexander von Humboldt International Conference on The Andes: Challenge for Geosciences*, Santiago de Chile, Chile, 28 November 2008, 41–49, <https://doi.org/10.5194/adgeo-22-41-2009>, 2009.
- 1220 Baraer, M., McKenzie, J., Mark, B. G., Gordon, R., Bury, J., Condom, T., Gomez, J., Knox, S., and Fortner, S. K.: Contribution of groundwater to the outflow from ungauged glacierized catchments: a multi-site study in the tropical Cordillera Blanca, Peru, *Hydrological Processes*, 29, 2561–2581, <https://doi.org/10.1002/hyp.10386>, 2015.
- Benettin, P., Bailey, S. W., Rinaldo, A., Likens, G. E., McGuire, K. J., and Botter, G.: Young runoff fractions control streamwater age and solute concentration dynamics, *Hydrological Processes*, 31, 2982–2986, <https://doi.org/10.1002/hyp.11243>, 2017.
- 1225 Blöschl, G., Bierkens, M. F. P., Chambel, A., Cudennee, C., Destouni, G., Fiori, A., Kirchner, J. W., McDonnell, J. J., Savenije, H. H. G., Sivapalan, M., Stump, C., Toth, E., Volpi, E., Carr, G., Lupton, C., Salinas, J., Széles, B., Viglione, A., Aksoy, H., Allen, S. T., Amin, A., Andréassian, V., Arheimer, B., Aryal, S. K., Baker, V., Bardsley, E., Barendrecht, M. H., Bartosova, A., Batelaan, O., Berghuijs, W. R., Beven, K., Blume, T., Bogaard, T., Borges de Amorim, P., Böttcher, M. E., Boulet, G., Breinl, K., Brilly, M., Brocca, L., Buytaert, W., Castellarin, A., Castelletti, A., Chen, X., Chen, Y., Chen, Y., Chiffard, P., Claps, P., Clark, M. P., Collins, A. L., Croke, B., Dathe, A., David, P. C., de Barros, F. P. J., de Rooij, G., Di 1230 Baldassarre, G., Driscoll, J. M., Duethmann, D., Dwivedi, R., Eris, E., Farmer, W. H., Feiccabrino, J., Ferguson, G., Ferrari, E., Ferraris, S., Fersch, B., Finger, D., Foglia, L., Fowler, K., Gartsman, B., Gascoin, S., Gaume, E., Gelfan, A., Geris, J., Gharari, S., Gleeson, T., Glendell, M., Gonzalez Bevacqua, A., González-Dugo, M. P., Grimaldi, S., Gupta, A. B., Guse, B., Han, D., Hannah, D., Harpold, A., Haun, S., Heal, K., Helfricht, K., Herrnegger, M., Hipsey, M., Hlaváčiková, H., Hohmann, C., Holko, L., Hopkinson, C., Hrachowitz, M., Illangasekare, T. H., Inam, A., Innocente, C., Istanbuloglu, E., 1235 Jarihani, B., et al.: Twenty three unsolved problems in hydrology (UPH) — a community perspective, *Hydrological Science Journal*, 64, 1141–1158, <https://doi.org/10.1080/02626667.2019.1620507>, 2019.
- Botter, G., Vingiani, F., Senatore, A., Jensen, C., Weiler, M., McGuire, K., Mendicino, G., and Durighetto, N.: Hierarchical climate-driven dynamics of the active channel length in temporary streams, *Scientific Reports*, 11, 21503, <https://doi.org/10.1038/s41598-021-00922-2>, 2021.
- 1240 Carroll, R. W. H., Bearup, L. A., Brown, W., Dong, W., Bill, M., and Willams, K. H.: Factors controlling seasonal groundwater and solute flux from snow-dominated basins, *Hydrological Processes*, 32, 2187–2202, <https://doi.org/10.1002/hyp.13151>, 2018.
- Carturan, L.: Replacing monitored glaciers undergoing extinction: a new measurement series on La Mare Glacier (Ortles-Cevedale, Italy), *Journal of Glaciology*, 62, 1093–1103, <https://doi.org/10.1017/jog.2016.107>, 2016.
- 1245 Carturan, L., Baroni, C., Becker, M., Bellin, A., Cainelli, O., Carton, A., Casarotto, C., Dalla-Fontana, G., Godio, A., Martinelli, T., Salvatore, M. C., and Seppi, R.: Decay of a long-term monitored glacier: Careser Glacier (Ortles-Cevedale, European Alps), *The Cryosphere*, 7, 1819–1838, <https://doi.org/10.5194/te-7-1819-2013>, 2013.

- Carturan, L., Baroni, C., Carton, A., Cazorzi, F., Fontana, G. D., Delpero, C., Salvatore, M. C., Seppi, R., and Zanoner, T.: Reconstructing fluctuations of la mare glacier (eastern Italian alps) in the late holocene: new evidence for a little ice age maximum around 1600 ad, *Geogr. Ann. Ser. Phys. Geogr.*, 96, 287–306, <https://doi.org/10.1111/geoa.12048>, 2014.
- 1250 Carturan, L., Zuecco, G., Seppi, R., Zanoner, T., Borga, M., Carton, A., and Dalla Fontana, G.: Catchment-Scale Permafrost Mapping using Spring Water Characteristics, *Permafr. Periglac. Process.*, 27, 253–270, <https://doi.org/10.1002/ppp.1875>, 2016.
- Carturan, L., De Blasi, F., Cazorzi, F., Zoecatelli, D., Bonato, P., Borga, M., and Dalla Fontana, G.: Relevance and Seale Dependence of Hydrological Changes in Glacierized Catchments: Insights from Historical Data Series in the Eastern Italian Alps, *Water*, 11, 89, <https://doi.org/10.3390/w11010089>, 2019.
- 1255 Ceperley, N., Zuecco, G., Beria, H., Carturan, L., Michelon, A., Penna, D., Larsen, J., and Schaeffli, B.: Seasonal snow cover decreases young water fractions in high Alpine catchments, *Hydrol. Process. Hydrological Processes*, 34, 4794–4813, <https://doi.org/10.1002/hyp.13937>, 2020.
- 1260 Chen, Z., Hartmann, A., Wagener, T., and Goldscheider, N.: Dynamics of water fluxes and storages in an Alpine karst catchment under current and potential future climate conditions, *Hydrol. Hydrology and Earth Syst. Sci., System Sciences*, 22, 3807–3823, <https://doi.org/10.5194/hess-22-3807-2018>, 2018.
- Christensen, C. W., Hayashi, M., and Bentley, L. R.: Hydrogeological characterization of an alpine aquifer system in the Canadian Rocky Mountains, *Hydrogeol. J.*, 28, 1871–1890, <https://doi.org/10.1007/s10040-020-02153-7>, 2020.
- 1265 Clark, M. P., Schaeffli, B., Schymanski, S. J., Samaniego, L., Luce, C. H., Jackson, B. M., Freer, J. E., Arnold, J. R., Moore, R. D., Istanbuloglu, E., and Ceola, S.: Improving the theoretical underpinnings of process-based hydrologic models, *Water Resources Research*, 52, 2350–2365, <https://doi.org/10.1002/2015WR017910>, 2016.
- Clow, D. W., Schrott, L., Webb, R., Campbell, D. H., Torizzo, A., and Dornblaser, M.: Ground Water Occurrence and Contributions to Streamflow in an Alpine Catchment, Colorado Front Range, *Groundwater*, 41, 937–950, <https://doi.org/10.1111/j.1745-6584.2003.tb02436.x>, 2003.
- 1270 Cochand, M., Christe, P., Ornstein, P., and Hunkeler, D.: Groundwater Storage in High Alpine Catchments and Its Contribution to Streamflow, *Water Resour. Res. Resources Research*, 55, 2613–2630, <https://doi.org/10.1029/2018WR022989>, 2019.
- 1275 Cowie, R. M., Knowles, J. F., Dailey, K. R., Williams, M. W., Mills, T. J., and Molotch, N. P.: Sources of streamflow along a headwater catchment elevational gradient, *J. Hydrol., Journal of Hydrology*, 549, 163–178, <https://doi.org/10.1016/j.jhydrol.2017.03.044>, 2017.
- Curran, J. H. and Biles, F. E.: Identification of Seasonal Streamflow Regimes and Streamflow Drivers for Daily and Peak Flows in Alaska, *Water Resour. Res.*, 57, e2020WR028425, <https://doi.org/10.1029/2020WR028425>, 2021.
- 1280 Déry, S. J., Stahl, K., Moore, R. D., Whitfield, P. H., Menounos, B., and Burford, J. E.: Detection of runoff timing changes in pluvial, nival, and glacial rivers of western Canada, *Water Resour. Res.*, 45, <https://doi.org/10.1029/2008WR006975>, 2009.

- Di Marco, N., Righetti, M., Avesani, D., Zaramella, M., Notarnicola, C., and Borga, M.: Comparison of MODIS and Model-Derived Snow-Covered Areas: Impact of Land Use and Solar Illumination Conditions, *20Geosciences*, *10*, 134, <https://doi.org/10.3390/geosciences10040134>, 2020.
- 1285 Dozier, J.: Spectral signature of alpine snow cover from the landsat thematic mapper, *Remote Sens. Environ., Sensing of Environment*, *28*, 9–22, [https://doi.org/10.1016/0034-4257\(89\)90101-6](https://doi.org/10.1016/0034-4257(89)90101-6), 1989.
- <https://doi.org/10.1007/s10661-019-7285-7>, 2019.
- 1290 Du, X., Fang, M., Lv, H., Cheng, T., Hong, P., and Liu, C.: Effect of snowmelt infiltration on groundwater recharge in a seasonal soil frost area: a case study in Northeast China, *Environ Monit Assess*, *191*, 151, <https://doi.org/10.1007/s10661-019-7285-7>, 2019.
- Duncan, H. P.: Baseflow separation – A practical approach, *J. Hydrol., Journal of Hydrology*, *575*, 308–313, <https://doi.org/10.1016/j.jhydrol.2019.05.040>, 2019.
- Durighetto, N., Mariotto, V., Zanetti, F., McGuire, K. J., Mendicino, G., Senatore, A., and Botter, G.: Probabilistic Description of Streamflow and Active Length Regimes in Rivers, *Water Resour. Res.*, *58*, e2021WR031344, <https://doi.org/10.1029/2021WR031344>, 2022.
- 1295 Engel, M., Penna, D., Bertoldi, G., Dell’Agnese, A., Soulsby, C., and Comiti, F.: Identifying run-off contributions during melt-induced run-off events in a glacierized alpine catchment, *Hydrol. Process., Hydrological Processes*, *30*, 343–364, <https://doi.org/10.1002/hyp.10577>, 2016.
- Farr, T. G., Rosen, P. A., Caro, E., Crippen, R., Duren, R., Hensley, S., Kobrick, M., Paller, M., Rodriguez, E., Roth, L., Seal, D., Shaffer, S., Shimada, J., Umland, J., Werner, M., Oskin, M., Burbank, D., and Alsdorf, D.: The Shuttle Radar Topography Mission, *Reviews of Geophysics*, *45*, <https://doi.org/10.1029/2005RG000183>, 2007.
- 1300 Flerchinger, G. N., Cooley, K. R., and Ralston, D. R.: Groundwater response to snowmelt in a mountainous watershed, *Journal of Hydrology*, *133*, 293–311, [https://doi.org/10.1016/0022-1694\(92\)90260-3](https://doi.org/10.1016/0022-1694(92)90260-3), 1992.
- von Freyberg, J., Allen, S. T., Seeger, S., Weiler, M., and Kirchner, J. W.: Sensitivity of young water fractions to hydro-climatic forcing and landscape properties across 22 Swiss catchments, *Hydrol. Hydrology and Earth Syst. Sci., System Sciences*, *22*, 3841–3861, <https://doi.org/10.5194/hess-22-3841-2018>, 2018.
- 1305 von Freyberg, J., Rüecker, A., Zappa, M., Schlumpf, A., Studer, B., and Kirchner, J. W.: Four years of daily stable water isotope data in stream water and precipitation from three Swiss catchments, *Sci. Data*, *9*, 46, <https://doi.org/10.1038/s41597-022-01148-1>, 2022.
- 1310 Frisbee, M. D., Phillips, F. M., Campbell, A. R., Liu, F., and Sanchez, S. A.: Streamflow generation in a large, alpine watershed in the southern Rocky Mountains of Colorado: Is streamflow generation simply the aggregation of hillslope runoff responses?, *Water Resour. Res.*, *47*, W06512, <https://doi.org/10.1029/2010WR009391>, 2011.
- Gallart, F., Valiente, M., Llorens, P., Cayuela, C., Sprenger, M., and Latron, J.: Investigating young water fractions in a small Mediterranean mountain catchment: Both precipitation forcing and sampling frequency matter, *Hydrol. Process., Hydrological Processes*, *34*, 3618–3634, <https://doi.org/10.1002/hyp.13806>, 20202020a.
- 1315 Gallart, F., von Freyberg, J., Valiente, M., Kirchner, J. W., Llorens, P., and Latron, J.: Technical note: An improved discharge sensitivity metric for young water fractions, *Hydrology and Earth System Sciences*, *24*, 1101–1107, <https://doi.org/10.5194/hess-24-1101-2020>, 2020b.

- Gascoin, S., Grizonnet, M., Bouchet, M., Salgues, G., and Hagolle, O.: Theia Snow collection: high-resolution operational snow cover maps from Sentinel-2 and Landsat-8 data, *Earth Syst. Sci. Data*, 11, 493–514, <https://doi.org/10.5194/essd-11-493-2019>, 2019.
- Gisolo, D., Previati, M., Bevilacqua, I., Canone, D., Boetti, M., Dematteis, N., Balocco, J., Ferrari, S., Gentile, A., Nsassila, M., Heery, B., Vereecken, H., and Ferraris, S.: A Calibration Free Radiation Driven Model for Estimating Actual Evapotranspiration of Mountain Grasslands (CLIME-MG), *J. Hydrol. Journal of Hydrology*, 610, 127948, <https://doi.org/10.1016/j.jhydrol.2022.127948>, 2022.
- 1325 Gleeson, T. and Manning, A. H.: Regional groundwater flow in mountainous terrain: Three-dimensional simulations of topographic and hydrogeologic controls, *Water Resour. Res.*, 44, W10403, <https://doi.org/10.1029/2008WR006848>, 2008.
- Gleeson, T., Moosdorf, N., Hartmann, J., and van Beek, L. P. H.: A glimpse beneath earth's surface: GLObal HYdrogeology MaPS (GLHYMPS) of permeability and porosity, *Geophys. Res. Lett.*, 41, 3891–3898, <https://doi.org/10.1002/2014GL059856>, 2014.
- Gordon, R. P., Lutz, L. K., McKenzie, J. M., Mark, B. G., Chavez, D., and Baraer, M.: Sources and pathways of stream generation in tropical proglacial valleys of the Cordillera Blanca, Peru, *J. Hydrol. Journal of Hydrology*, 522, 628–644, <https://doi.org/10.1016/j.jhydrol.2015.01.013>, 2015.
- 1335 [Gorelick, N., Hancher, M., Dixon, M., Ilyushchenko, S., Thau, D., and Moore, R.: Google Earth Engine: Planetary-scale geospatial analysis for everyone, *Remote Sensing of Environment*, 202, 18–27, <https://doi.org/10.1016/j.rse.2017.06.031>, 2017.](#)
- Goulden, M. L., Anderson, R. G., Bales, R. C., Kelly, A. E., Meadows, M., and Winston, G. C.: Evapotranspiration along an elevation gradient in California's Sierra Nevada, *J. Geophys. Res. Biogeosciences*, 117, G03028, <https://doi.org/10.1029/2012JG002027>, 2012.
- 1340 Guastini, E., Zuecco, G., Errico, A., Castelli, G., Bresci, E., Preti, F., and Penna, D.: How does streamflow response vary with spatial scale? Analysis of controls in three nested Alpine catchments, *J. Hydrol.*, 570, 705–718, <https://doi.org/10.1016/j.jhydrol.2019.01.022>, 2019.
- Hall, F. R.: Base Flow Recessions—A Review, *Water Resour. Res.*, 4, 973–983, <https://doi.org/10.1029/WR004i005p00973>, 1968.
- 1345 Harrington, J. S., Mozil, A., Hayashi, M., and Bentley, L. R.: Groundwater flow and storage processes in an inactive rock glacier, *Hydrol. Processes: Hydrological Processes*, 32, 3070–3088, <https://doi.org/10.1002/hyp.13248>, 2018.
- Harrison, H. N., Hammond, J. C., Kampf, S., and Kiewiet, L.: On the hydrological difference between catchments above and below the intermittent-persistent snow transition, *Hydrol. Processes: Hydrological Processes*, 35, e14411, <https://doi.org/10.1002/hyp.14411>, 2021.
- 1350 Hayashi, M.: Alpine Hydrogeology: The Critical Role of Groundwater in Sourcing the Headwaters of the World, *Ground Water*, 58, 498–510, <https://doi.org/10.1111/gwat.12965>, 2020.
- Hofmeister, F., Arias-Rodriguez, L. F., Premier, V., Marin, C., Notarnicola, C., Disse, M., and Chiogna, G.: Intercomparison of Sentinel-2 and modelled snow cover maps in a high-elevation Alpine catchment, *J. Hydrol. Journal of Hydrology*, X, 15, 100123, <https://doi.org/10.1016/j.hydroa.2022.100123>, 2022.

- 1355 [Jansson, P., Hock, R., and Schneider, T.: The concept of glacier storage: a review, *Journal of Hydrology*, 282, 116–129, \[https://doi.org/10.1016/S0022-1694\\(03\\)00258-0\]\(https://doi.org/10.1016/S0022-1694\(03\)00258-0\), 2003.](#)
- Jasechko, S.: Global Isotope Hydrogeology—Review, [Rev.—Geophys.,Reviews of Geophysics](#), 57, 835–965, <https://doi.org/10.1029/2018RG000627>, 2019.
- 1360 Jasechko, S., Kirchner, J. W., Welker, J. M., and McDonnell, J. J.: Substantial proportion of global streamflow less than three months old, [Nat.—Geosci.,Nature Geoscience](#), 9, 126–129, <https://doi.org/10.1038/ngeo2636>, 2016.
- [Jeníček, M., Seibert, J., and Staudinger, M.: Modeling of Future Changes in Seasonal Snowpack and Impacts on Summer Low Flows in Alpine Catchments, *Water Resour. Res.*, 54, 538–556, <https://doi.org/10.1002/2017WR021648>, 2018.](#)
- [Käser, D. and Hunkeler, D.: Contribution of alluvial groundwater to the outflow of mountainous catchments, *Water Resour. Res.—Resources Research*, 52, 680–697, <https://doi.org/10.1002/2014WR016730>, 2016.](#)
- 1365 [Keller, D. E., Fischer, A. M., Liniger, M. A., Appenzeller, C., and Knutti, R.: Testing a weather generator for downscaling climate change projections over Switzerland, *Int.—J.—Climatol.,International Journal of Climatology*, 37, 928–942, <https://doi.org/10.1002/joc.4750>, 2017.](#)
- [Kirchner, J. W.: A double paradox in catchment hydrology and geochemistry, *Hydrol. Process.*, 17, 871–874, <https://doi.org/10.1002/hyp.5108>, 2003.](#)
- 1370 [Kirchner, J. W.: Aggregation in environmental systems-Part 1: Seasonal tracer cycles quantify young water fractions, but not mean transit times, in spatially heterogeneous catchments, *Hydrol.—Hydrology and Earth Syst.—Sci.,System Sciences*, 20, 279–297, <https://doi.org/10.5194/hess-20-279-2016>, 2016a.](#)
- [Kirchner, J. W.: Aggregation in environmental systems-Part 2: Catchment mean transit times and young water fractions under hydrologic nonstationarity, *Hydrol.—Hydrology and Earth Syst.—Sci.,System Sciences*, 20, 299–328, <https://doi.org/10.5194/hess-20-299-2016>, 2016b.](#)
- 1375 [Li, L., Sullivan, P. L., Benettin, P., Cirpka, O. A., Bishop, K., Brantley, S. L., Knapp, J. L. A., van Meerveld, I., Rinaldo, A., Seibert, J., Wen, H., and Kirchner, J. W.: Toward catchment hydro-biogeochemical theories, *WIREs Water*, 8, e1495, <https://doi.org/10.1002/wat2.1495>, 2021.](#)
- [Liu, F., Williams, M. W., and Caine, N.: Source waters and flow paths in an alpine catchment, Colorado Front Range, United States, *Water Resour.—Res.—Resources Research*, 40, <https://doi.org/10.1029/2004WR003076>, 2004.](#)
- 1380 [Lucianetti, G., Penna, D., Mastroiillo, L., and Mazza, R.: The Role of Snowmelt on the Spatio-Temporal Variability of Spring Recharge in a Dolomitic Mountain Group, Italian Alps, *Water*, 12, 2256, <https://doi.org/10.3390/w12082256>, 2020.](#)
- [Lutz, S. R., Krieg, R., Müller, C., Zink, M., Knöller, K., Samaniego, L., and Merz, R.: Spatial Patterns of Water Age: Using Young Water Fractions to Improve the Characterization of Transit Times in Contrasting Catchments, *Water Resour.—Res.—Resources Research*, 54, 4767–4784, <https://doi.org/10.1029/2017WR022216>, 2018.](#)
- 1385 [Lyne, V. and Hollick, M.: Stochastic Time-Variable Rainfall-Runoff Modeling, *Institution of Engineers Australia National Conference*, 89–92, 1979.](#)
- [Martin, C., Kampf, S. K., Hammond, J. C., Wilson, C., and Anderson, S. P.: Controls on Streamflow Densities in Semiarid Rocky Mountain Catchments, *Water*, 13, 521, <https://doi.org/10.3390/w13040521>, 2021.](#)

- 1390 Martinec, J.: Subsurface flow from snowmelt traced by tritium, *Water Resour. Res.*, **11**, 496–498, <https://doi.org/10.1029/WR011i003p00496>, 1975.
- McDonnell, J. J.: Are all runoff processes the same?, *Hydrol. Process.*, **27**, 4103–4111, <https://doi.org/10.1002/hyp.10076>, 2013.
- McDonnell, J. J.: Beyond the water balance, *Nat. Nature Geosci.*, **10**, 396–396, <https://doi.org/10.1038/ngeo2964>, 2017.
- 1395 McDonnell, J. J., Spence, C., Karran, D. J., van Meerveld, H. J. (Hja), and Harman, C. J.: Fill and Spill: A Process Description of Runoff Generation at the Scale of the Beholder, *Water Resour. Res.*, **57**, e2020WR027514, <https://doi.org/10.1029/2020WR027514>, 2021.
- 1400 Michelon, A., Ceperley, N., Beria, H., Larsen, J., Vennemann, T., and Schaefli, B.: Studying the dynamic of a high alpine catchment based on multiple natural tracers, *Hydrol. Hydrology and Earth Syst. Sci. Discuss. System Sciences Discussions*, **1–43**, <https://doi.org/10.5194/hess-2022-48>, 2022.
- Moore, R. D. (Dan), Trubilowicz, J. w., and Buttle, J. m: Prediction of Streamflow Regime and Annual Runoff for Ungauged Basins Using a Distributed Monthly Water Balance Model, *JAWRA J. Am. Water Resour. Assoc.*, **48**, 32–42, <https://doi.org/10.1111/j.1752-1688.2011.00595.x>, 2012.
- Pardè, M.: Fleuves et rivières, Librairie Armand Colin, Paris, 1933.
- 1405 Paznekas, A. and Hayashi, M.: Groundwater contribution to winter streamflow in the Canadian Rockies, *Can. Water Resour. J. Rev. Can. Ressour. Hydr.*, **41**, 484–499, <https://doi.org/10.1080/07011784.2015.10660870>, 2016.
- Müller, T., Lane, S. N., and Schaefli, B.: Towards a hydrogeomorphological understanding of proglacial catchments: review of current knowledge and assessment of groundwater storage and release in an Alpine catchment, *Hydrology and Earth System Sciences Discussions*, **1–45**, <https://doi.org/10.5194/hess-2022-110>, 2022.
- 1410 Nathan, R. J. and McMahon, T. A.: Evaluation of automated techniques for base flow and recession analyses, *Water Resources Research*, **26**, 1465–1473, <https://doi.org/10.1029/WR026i007p01465>, 1990.
- Painter, K. J., Gentile, A., and Ferraris, S.: A stochastic cellular automaton model to describe the evolution of the snow-covered area across a high-elevation mountain catchment, *Science of The Total Environment*, **857**, 159195, <https://doi.org/10.1016/j.scitotenv.2022.159195>, 2023.
- 1415 Pavlovskii, I., Hayashi, M., and Lennon, M. R.: Transformation of snow isotopic signature along groundwater recharge pathways in the Canadian Prairies, *Journal of Hydrology*, **563**, 1147–1160, <https://doi.org/10.1016/j.jhydrol.2017.09.053>, 2018.
- 1420 Penna, D., van Meerveld, H. J., Zuecco, G., Dalla Fontana, G., and Borga, M.: Hydrological response of an Alpine catchment to rainfall and snowmelt events, *J. Hydrol., Journal of Hydrology*, **537**, 382–397, <https://doi.org/10.1016/j.jhydrol.2016.03.040>, 2016.
- Penna, D., Engel, M., Bertoldi, G., and Comiti, F.: Towards a tracer-based conceptualization of meltwater dynamics and streamflow response in a glacierized catchment, *Hydrol. Earth Syst. Sci.*, **21**, 23–41, <https://doi.org/10.5194/hess-21-23-2017>, 2017.

- 1425 Petersky, R. and Harpold, A.: Now you see it, now you don't: a case study of ephemeral snowpacks and soil moisture response in the Great Basin, USA, *Hydrology and Earth Syst. Sci., System Sciences*, 22, 4891–4906, <https://doi.org/10.5194/hess-22-4891-2018>, 2018.
- Piccolroaz, S., Calamita, E., Majone, B., Gallice, A., Siviglia, A., and Toffolon, M.: Prediction of river water temperature: a comparison between a new family of hybrid models and statistical approaches, *Hydrological Processes*, 30, 3901–3917, <https://doi.org/10.1002/hyp.10913>, 2016.
- 1430 Rey, D. M., Hinckley, E.-L. S., Walvoord, M. A., and Singha, K.: Integrating observations and models to determine the effect of seasonally frozen ground on hydrologic partitioning in alpine hillslopes in the Colorado Rocky Mountains, USA, *Hydrological Processes*, 35, e14374, <https://doi.org/10.1002/hyp.14374>, 2021.
- Saberi, L., McLaughlin, R. T., Ng, G.-H. C., La Frenierre, J., Wickert, A. D., Baraer, M., Zhi, W., Li, L., and Mark, B. G.: Multi-scale temporal variability in meltwater contributions in a tropical glacierized watershed, *Hydrology and Earth Syst. Sci., System Sciences*, 23, 405–425, <https://doi.org/10.5194/hess-23-405-2019>, 2019.
- 1435 Santos, A. C., Portela, M. M., Rinaldo, A., and Schaeffli, B.: Analytical flow duration curves for summer streamflow in Switzerland, *Hydrology and Earth Syst. Sci., System Sciences*, 22, 2377–2389, <https://doi.org/10.5194/hess-22-2377-2018>, 2018.
- 1440 Scherler, M., Hauck, C., Hoelzle, M., Stähli, M., and Völksch, I.: Meltwater infiltration into the frozen active layer at an alpine permafrost site, *Permafrost and Periglacial Processes*, 21, 325–334, <https://doi.org/10.1002/ppp.694>, 2010.
- Schmieder, J., Seeger, S., Weiler, M., and Strasser, U.: 'Teflon Basin' or Not? A High-Elevation Catchment Transit Time Modeling Approach, *Hydrology*, 6, 92, <https://doi.org/10.3390/hydrology6040092>, 2019.
- Somers, L. D. and McKenzie, J. M.: A review of groundwater in high mountain environments, *WIREs Water*, 7, e1475, <https://doi.org/10.1002/wat2.1475>, 2020.
- 1445 Somers, L. D., McKenzie, J. M., Mark, B. G., Lagos, P., Ng, G.-H. C., Wickert, A. D., Yarleque, C., Baraer, M., and Silva, Y.: Groundwater Buffers Decreasing Glacier Melt in an Andean Watershed—But Not Forever, *Geophys. Res. Lett., Geophysical Research Letters*, 46, 13016–13026, <https://doi.org/10.1029/2019GL084730>, 2019.
- 1450 Staudinger, M. and Seibert, J.: Predictability of low flow—An assessment with simulation experiments, *J. Hydrol.*, 519, 1383–1393, <https://doi.org/10.1016/j.jhydrol.2014.08.061>, 2014.
- Staudinger, M., Weiler, M., and Seibert, J.: Quantifying sensitivity to droughts—an experimental modeling approach, *Hydrology and Earth Syst. Sci.*, 19, 1371–1384, <https://doi.org/10.5194/hess-19-1371-2015>, 2015.
- Staudinger, M., Stoelzle, M., Seeger, S., Seibert, J., Weiler, M., and Stahl, K.: Catchment water storage variation with elevation, *Hydrological Processes*, 31, 2000–2015, <https://doi.org/10.1002/hyp.11158>, 2017.
- 1455 Staudinger, M., Seeger, S., Herbstritt, B., Stoelzle, M., Seibert, J., Stahl, K., and Weiler, M.: The CH-IRP data set: a decade of fortnightly data on $\delta^2\text{H}$ and $\delta^{18}\text{O}$ in streamflow and precipitation in Switzerland, *Earth Syst. Sci., System Science Data*, 12, 3057–3066, <https://doi.org/10.5194/essd-12-3057-2020>, 2020.
- Stockinger, M., Reemt Bogena, H., Lücke, A., Stumpp, C., and Vereecken, H.: Time variability and uncertainty in the fraction of young water in a small headwater catchment, *Hydrology and Earth Syst. Sci., System Sciences*, 23, 4333–4347, <https://doi.org/10.5194/hess-23-4333-2019>, 2019.

- 1460 Tromp van Meerveld, H. J. and McDonnell, J. J.: Threshold relations in subsurface stormflow: 1. A 147-storm analysis of the Panola hillslope, *Water Resour. Res.*, 42, <https://doi.org/10.1029/2004WR003778>, 2006.
Stockinger, M. P., Bogena, H. R., Lücke, A., Diekkrüger, B., Cornelissen, T., and Vereecken, H.: Tracer sampling frequency influences estimates of young water fraction and streamwater transit time distribution, *Journal of Hydrology*, 541, 952–964, <https://doi.org/10.1016/j.jhydrol.2016.08.007>, 2016.
- 1465 Stoelzle, M., Schuetz, T., Weiler, M., Stahl, K., and Tallaksen, L. M.: Beyond binary baseflow separation: a delayed-flow index for multiple streamflow contributions, *Hydrology and Earth System Sciences*, 24, 849–867, <https://doi.org/10.5194/hess-24-849-2020>, 2020.
 Weingartner, R. and Aschwanden, H.: Abflussregimes als Grundlage zur Abschätzung von Mittelwerten des Abflusses, *Hydrol. Atlas Hydrologischer atlas der Schweiz*, Tafel 5.2, 1992.
- 1470 Williams, M. W., Wilson, A., Tshering, D., Thapa, P., and Kayastha, R. B.: Using geochemical and isotopic chemistry to evaluate glacier melt contributions to the Chamkar Chhu (river), Bhutan, *Ann. Glaciol., Annals of Glaciology*, 57, 339–348, <https://doi.org/10.3189/2016AoG71A068>, 2016.
Wilson, A. M., Williams, M. W., Kayastha, R. B., and Racoviteanu, A.: Use of a hydrologic mixing model to examine the roles of meltwater, precipitation and groundwater in the Langtang River basin, Nepal, *Ann. Glaciol., Annals of Glaciology*, 57, 155–168, <https://doi.org/10.3189/2016AoG71A067>, 2016.
- 1475 Zuecco, G., PennaWilusz, D. C., Harman, C. J., and Borga, M.: Runoff generation in mountain catchments: long-term hydrological monitoring in the Rio Vauz Ball, W. P.: Sensitivity of Catchment, Italy, *Cuad. Investig. Geográfica*, 44, 397–428, <https://doi.org/10.18172/eig.3327>, 2018.
Zuecco, G., Carturan, L., De Blasi, F., Seppi, R., Zanoner, T., Penna, D., Borga, M., Carton, A., Dalla Fontana, G.: Understanding hydrological processes in glacierized catchments: Evidence and implications of highly variable isotopic and electrical conductivity data, *Hydrol. Process.*, 33, 816–832 *Future Climates, Water Resources Research*, 53, 10231–10256, <https://doi.org/10.1002/hyp.13366>, 20192017WR020894, 2017.